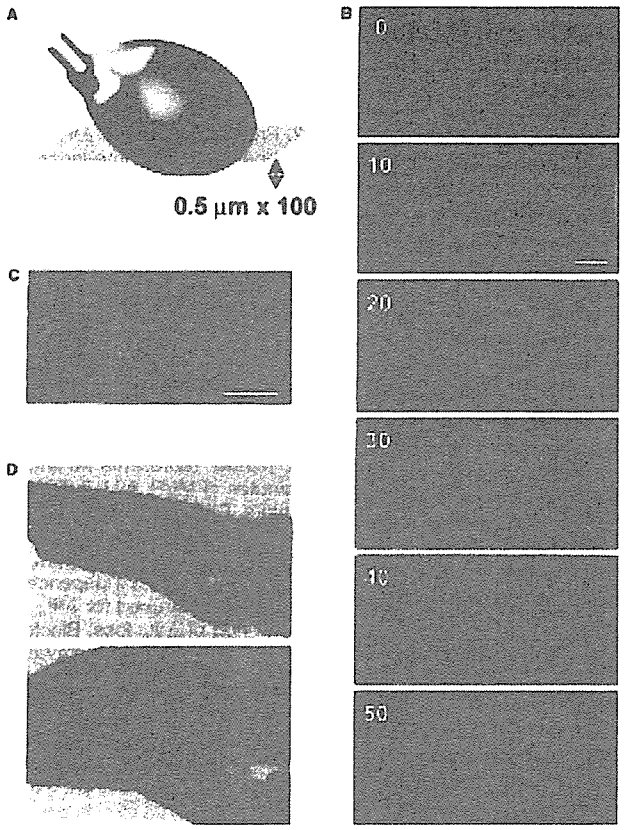

Figure 1. Two dimensional and 3-dimensional imaging of mitochondria in perfused rat hearts. A, Schematic drawing of the perfused heart and optical slices. The images were obtained every 0.5 μm ×100 slices. B, Representative optical slices of TMRE-loaded heart obtained at various depths. Numbers indicate depth (in micrometers) from the epicardial surface. Scale bar=20 μm. C, Zoomed image (×3) showing individual mitochondria. Scale bar=10 μm. D, Three-dimensional processing images of a single cardiomyocyte.

period of latency that varied from cell to cell, after which $\Delta\Psi_m$ started to decrease. Once it began, this rapid loss of $\Delta\Psi_m$ was complete within 5 minutes, and it was irreversible. Figure 2C shows the time courses of representative cells undergoing the collapse of $\Delta\Psi_m$, monitored at 1-minute intervals. The kinetics of $\Delta\Psi_m$ loss during the ischemic period (solid lines) were identical to those during the reperfusion period (dashed lines). Here, "ischemic period" represents MI and the first 30 minutes of MI/R. Summarized data of duration of $\Delta\Psi_m$ loss in each cell are shown in Figure 2D; "duration" was defined as the time required for 50% loss of TMRE fluorescence in this analysis. The durations of $\Delta\Psi_m$ loss were comparable between the ischemic and reperfusion periods, which suggests a common underlying mechanism. Figure 2E shows that the duration of $\Delta\Psi_m$ loss did not vary with latency in any given cell: $\Delta\Psi_m$ dissipation occurred within 5 minutes, regardless of the delay with which it began.

In Figure 3, a representative cell undergoing $\Delta\Psi_m$ loss is shown. These 1-minute interval images suggest that $\Delta\Psi_m$ loss was proceeding almost homogeneously throughout the cell, but it never affected the neighboring cells (Figure 3A). This was confirmed by a quantitative assessment (Figure 3B; line scan shown in the middle, and fluorescence time course of individual cells shown on the right). To further investigate the time-dependent changes of $\Delta\Psi_m$ loss in a single cell with higher spatiotemporal resolution, time-lapse images were taken every 10 seconds (Figure 4A; online Data Supplement, Movie V). $\Delta\Psi_m$ loss was initiated in a particular area of mitochondria (Figure 4B, right, white arrowhead), and it rapidly propagated along the longitudinal axis within the cell (Figure 4B, middle panel, white arrows). The calculated velocity of the $\Delta\Psi_m$ loss propagation was 2.2 μm/s, which was comparable to a previously reported propagation rate of the mitochondrial apoptotic signal in H9c2 cells.[15]

We confirmed that cells that underwent $\Delta\Psi_m$ loss eventually experienced cytolysis, as evidenced by the fluorescent indicators BCECF-AM and PI. As shown in Figure 5, a cell with $\Delta\Psi_m$ loss was PI-positive (left; white arrows) and showed leakage of BCECF (middle), indicating cytolysis. Meanwhile, a cell with intact $\Delta\Psi_m$ was PI-negative (left; white arrowhead) and showed no leakage of BCECF.

A key mechanism of $\Delta\Psi_m$ loss is by the opening of the mitochondrial permeability transition pore (MPTP), a nonspecific pore that opens at the contact site between outer and inner mitochondrial membranes.[5] We have confirmed in an isolated cardiomyocyte model that $\Delta\Psi_m$ loss is mediated by the MPTP opening.[7] Accordingly, we tested the effect of an MPTP blocker, CsA,[16] in this system. CsA (0.2 or 1.0 μmol/L) blocked the rapid dissipation of $\Delta\Psi_m$, but the cells appeared to lose $\Delta\Psi_m$ with slower kinetics (Figure 6A, CsA 0.2 and CsA 1.0; online Data Supplement Movies VI and VII). The time course of fluorescence obtained from 10 representative cells (Figure 6B) indicates prolonged duration of $\Delta\Psi_m$ loss and smaller cellular heterogeneity in the CsA-treated group. Finally, we tested the effect of IPC. IPC is an endogenous mechanism whereby brief periods of ischemia and reperfusion paradoxically protect the myocardium against the damaging effects of subsequent prolonged ischemia.[17] IPC decreased the number of cells undergoing $\Delta\Psi_m$ loss (Figure 6A, IPC; Movie VIII), whereas it did not change the duration of $\Delta\Psi_m$ loss in unprotected cells. Moreover, $\Delta\Psi_m$ level was fully polarized in the protected cells (Figure 6B). Figure 6C shows the average of TMRE fluorescence intensity at the end of the experimental period (60 minutes) from 10 randomly and prospectively selected cells in each group. The $\Delta\Psi_m$-preserving effect of CsA 0.2 and IPC was remarkable, but that of CsA 1.0 was less and was modest. Although CsA 0.2 and IPC achieved a similar level of protection (Figure 6C), the mechanism of action was suggested to be distinct, as evidenced by the differential kinetics of $\Delta\Psi_m$ loss in each individual cell (Figure 6B). The duration of $\Delta\Psi_m$ loss was much longer in the CsA 0.2 group than in the MI/R and IPC groups (Figure 6D). Moreover, IPC significantly delayed the onset of $\Delta\Psi_m$ loss, whereas CsA did not (Figure 6E). The wave velocity of $\Delta\Psi_m$ loss propagation in the IPC group was 1.9 μm/s, which was comparable to that of the MI/R (IPC absent) group.

Discussion

Visualization of Living Mitochondria in the Perfused Heart With TPLSM

This is the first demonstration of living mitochondria in perfused hearts and their responses to ischemia/reperfusion. The impor-

Downloaded from circ.ahajournals.org at KYOTO UNIV Igaku Toshokan on April 3, 2007

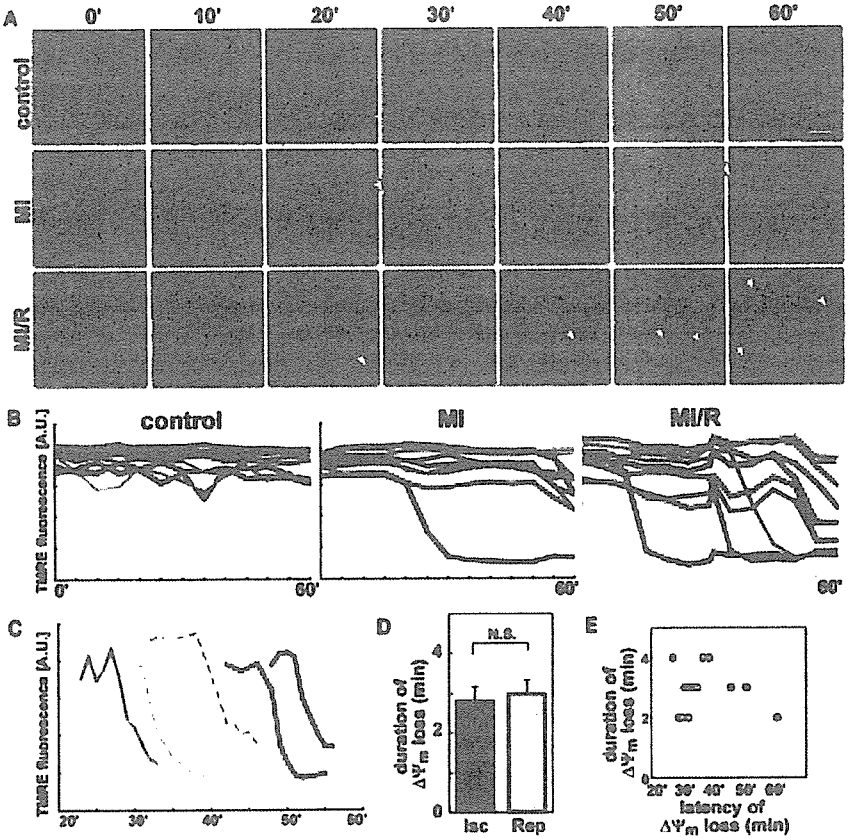

Figure 2. Progressive loss of $\Delta\Psi_m$ during ischemia/reperfusion. A, Time-lapse images taken every 5 minutes. Control indicates control perfusion for 60 minutes. Data are from a single experiment, representative of at least 3 independent experiments. Scale bar=50 μm. B, Time course of TMRE fluorescence in each individual cell, monitored at 5-minute intervals. C, Time course of TMRE fluorescence in representative cells undergoing $\Delta\Psi_m$ loss, monitored at 1-minute intervals. Solid lines indicate ischemic period; dashed lines, reperfusion period. "Ischemic period" represents MI and the first 30 minutes of MI/R. A.U. indicates arbitrary units. D, Summarized data of the duration required for $\Delta\Psi_m$ loss in the ischemic period (Isc) and the reperfusion period (Rep); n=6, from 3 independent scans. E, Duration required for $\Delta\Psi_m$ loss vs latency period of $\Delta\Psi_m$ loss. Black circles indicate ischemic period; gray circles, reperfusion period; and line, regression line, indicating no correlation between duration and latency of $\Delta\Psi_m$ loss.

tance of the detection of cell death processes at the subcellular level in the heart in situ has attracted attention,[18,19] especially when compared with conventional studies, which depend on rough end points such as myocardial enzyme release, recovery of left ventricular pressure, or macroscopic measurement of infarct size. TPLSM is ideal for bioimaging of the intact heart and has been used in pioneering studies by Rubart et al.[20,21]

Real-Time Monitoring of Mitochondrial Function During Ischemia/Reperfusion

Taking advantage of this novel imaging system, we monitored real-time mitochondrial function under MI/R at the single cardiomyocyte level, or single mitochondrion level. Our observations provide important insights into the understanding of ischemia/reperfusion injury.

Kinetics and Mechanisms of $\Delta\Psi_m$ Loss

During ischemia/reperfusion, cells maintained a constant $\Delta\Psi_m$ for the cell-to-cell specific period of latency, followed by a rapid, complete, and irreversible depolarization of $\Delta\Psi_m$. Once initiated, the duration of $\Delta\Psi_m$ depolarization was constant and did not depend on the length of the latency. The kinetics of $\Delta\Psi_m$ loss appeared almost identical between ischemia and reperfusion, which suggests a common mechanism. Considering the similar

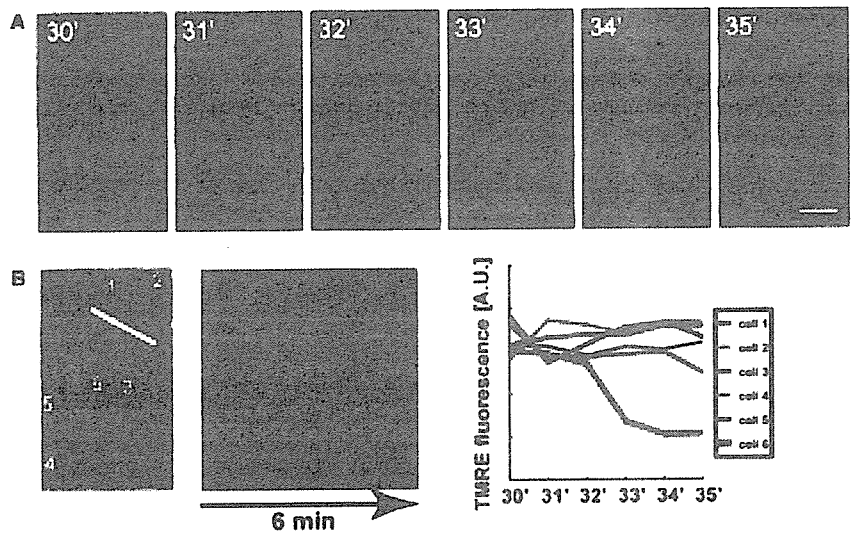

Figure 3. Intercellular propagation of $\Delta\Psi_m$ loss. A, Time-lapse images were taken every 1 minute. Representative scan of the MI/R group (30 minutes of ischemia followed by 30 minutes of reperfusion). Scale bar=20 μm. B, Middle, Time-line image of TMRE fluorescence by analysis of a white line drawn in the left panel; right, time course of TMRE fluorescence in each individual cell numbered in the left panel. A.U. indicates arbitrary units.

Downloaded from circ.ahajournals.org at KYOTO UNIV Igaku Toshokan on April 3, 2007

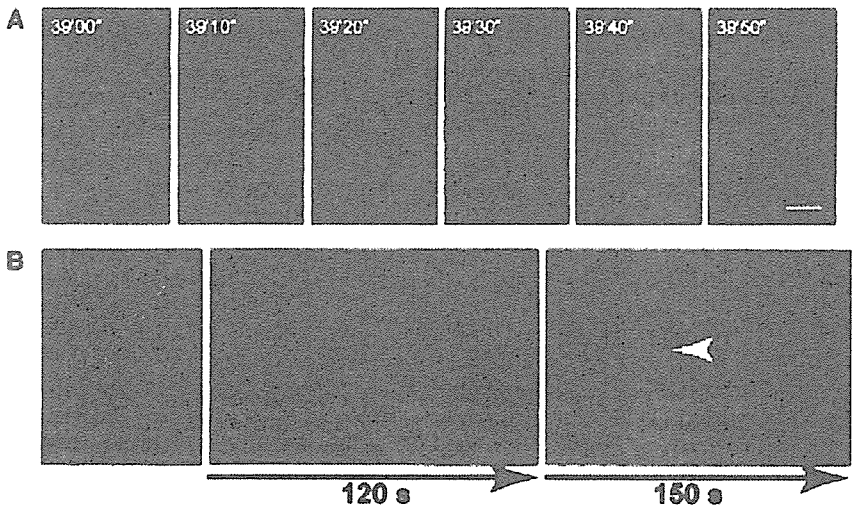

Figure 4. Intracellular propagation of $\Delta\Psi_m$ loss. A, Time-lapse images were taken every 10 seconds. Representative scan of the MI group (60 minutes of ischemia). Scale bar=10 μm. B, Middle, Time-line image of TMRE fluorescence by analysis of a white dashed line drawn in the left panel. White arrow indicates propagation of $\Delta\Psi_m$ loss starting from a particular area of mitochondria; right, time-area montage image of TMRE fluorescence by analysis of a white open box drawn in the left panel. White arrowhead indicates the single mitochondrion where propagation of $\Delta\Psi_m$ loss appeared to start.

kinetics of $\Delta\Psi_m$ loss demonstrated in our previous study with isolated cardiomyocytes,[7] the opening of the MPTP is most likely involved in the mitochondrial collapse during ischemia as well as reperfusion. CsA, a potent MPTP blocker, showed partial protective effects against ischemia/reperfusion–induced $\Delta\Psi_m$ loss. Although a potent MPTP inhibitor in isolated mitochondria, the effect of CsA is inconsistent in intact cells.[22] In addition, CsA is not completely specific and inhibits calcineurin, which also plays an important role in modulating mitochondrial death signals.[23] Further studies are required to elucidate the mechanisms of $\Delta\Psi_m$ loss.

Cell Death During Ischemia and Reperfusion

There was progressive $\Delta\Psi_m$ loss during the ischemic period and a more prominent $\Delta\Psi_m$ loss on reperfusion. Obviously, permanent ischemia eventually kills all the cells, and reperfusion is necessary to salvage them. However, during reperfusion, the heart undergoes further damage due in large part to the generation of reactive oxygen species.[24] Many drugs have been shown to reduce infarct size when administered before ischemia, but it was recently reported that cytochrome P450 inhibitors administered at reperfusion reduced infarct size.[25] Our observations in the present study support the possibility that therapies directed at inhibiting mitochondrial dysfunction and resultant cell death could be successful even if applied during resumption of coronary blood flow.

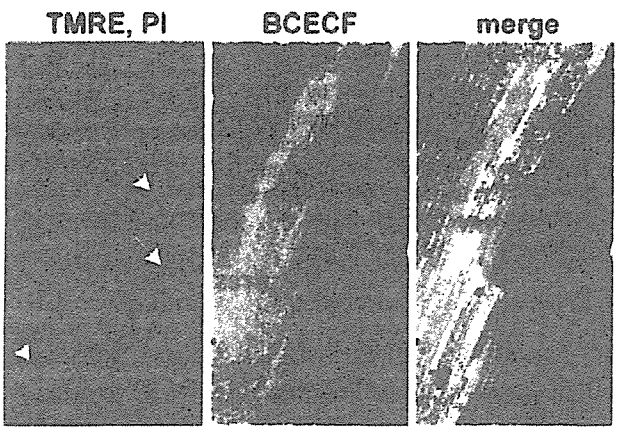

Figure 5. $\Delta\Psi_m$ loss followed by cytolysis. Images were taken at the end of 30 minutes of ischemia followed by 30 minutes of reperfusion. Red channel shows TMRE and PI (left); green channel shows BCECF (middle); and merged image (right).

Cellular and Subcellular Heterogeneity of Mitochondrial Function

Interestingly, $\Delta\Psi_m$ loss was initiated sporadically, and it did not affect neighboring cells, which suggests closure of the gap junction before $\Delta\Psi_m$ loss. At the subcellular level, $\Delta\Psi_m$ loss was initiated in a particular area of mitochondria and rapidly propagated along the longitudinal axis within the cell. These cellular and subcellular dispersions of the $\Delta\Psi_m$ level after ischemia/reperfusion can lead to spatiotemporal heterogeneity of excitability in the heart. Recently, Akar and colleagues[26] demonstrated that this heterogeneity may underlie the genesis of potentially lethal cardiac arrhythmias. In the present study, the hearts were perfused with buffer containing 10 mmol/L BDM to halt contraction. BDM reportedly has a cardioprotective effect.[27] The closure of the gap junction mediated by BDM[28] may potentially underlie its cardioprotective property,[29] but we confirmed that sporadic $\Delta\Psi_m$ loss was similarly observed in the absence of BDM (data not shown), which indicates that sporadic $\Delta\Psi_m$ loss and the resultant mitochondrial heterogeneity were not an effect of BDM. This was further confirmed by the similar sequence of events observed under perfusion with cytochalasin D (50 μmol/L), which uncouples excitation/contraction.

Strategies Toward Cardioprotection

This imaging system can be used to assess potential therapeutic agents for ameliorating myocardial infarction. Indeed, the feasibility of the system was confirmed by the remarkable cardioprotective effect of IPC and CsA. IPC not only decreased the number of cells undergoing $\Delta\Psi_m$ loss but also delayed the onset of $\Delta\Psi_m$ loss (Figure 6E), whereas it changed neither the duration of $\Delta\Psi_m$ loss (Figure 6D) nor the intracellular wave propagation velocity of $\Delta\Psi_m$ loss in unprotected cells. IPC fully preserved the $\Delta\Psi_m$ level in protected cells. CsA, in contrast, did not change the latency period (Figure 6E) but did slow the process of $\Delta\Psi_m$ loss (Figure 6D), and all the cells were partially depolarized.

Downloaded from circ.ahajournals.org at KYOTO UNIV Igaku Toshokan on April 3, 2007

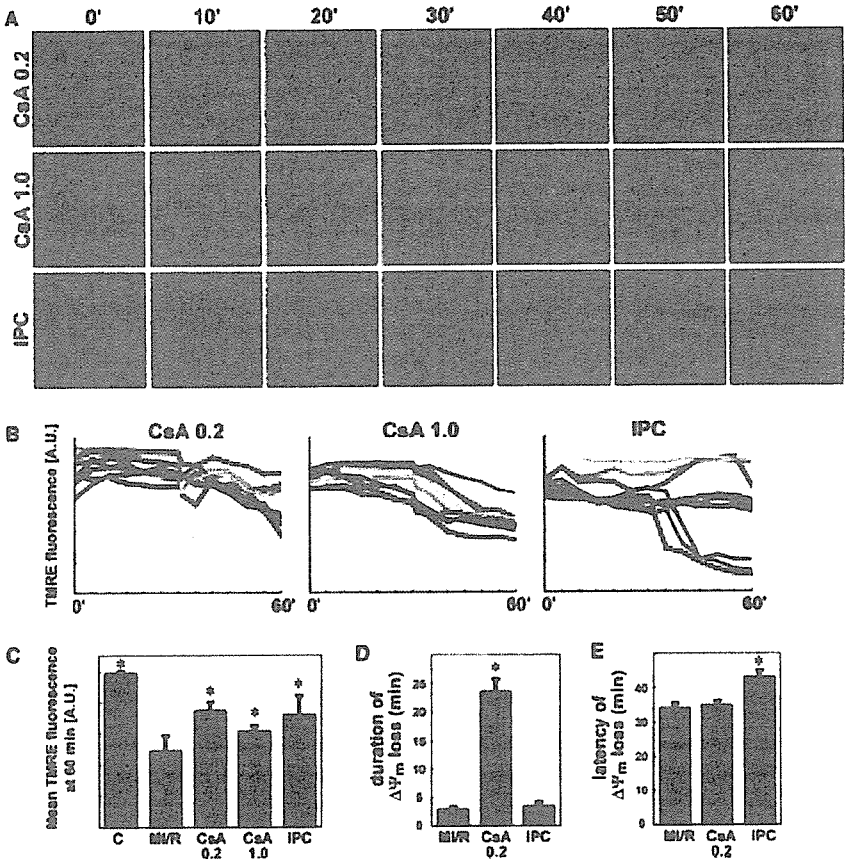

Figure 6. Effects of CsA and IPC. A, Time-lapse images taken every 5 minutes. CsA indicates infusion of 0.2 or 1.0 μmol/L CsA, followed by 30 minutes of ischemia and 30 minutes of reperfusion. IPC indicates 3 cycles of 5 minutes of ischemia and 5 minutes of reperfusion, followed by 30 minutes of ischemia and 30 minutes of reperfusion. Data are from a single experiment, representative of at least 3 independent experiments. Scale bar=50 μm. B, Time course of TMRE fluorescence in each individual cell, monitored at 5-minute intervals. C, Mean fluorescence intensity at the end of the experimental period (60 minutes) from 10 cells randomly and prospectively selected in each group. *$P<0.05$ vs MI/R. D, Duration required for $\Delta\Psi_m$ loss in each group. *$P<0.05$ vs MI/R. E, Latency period of $\Delta\Psi_m$ loss in each group. *$P<0.05$ vs MI/R. A.U. indicates arbitrary units.

Therefore, cellular heterogeneity was much greater in the IPC-treated group than in the CsA-treated group. The slower $\Delta\Psi_m$ loss observed in the CsA group may be mediated by a partial (or low-conductance) opening of the MPTP or by another mechanism that comes into play under the inhibition of the MPTP, but further studies are needed to confirm this. Collectively, CsA and IPC may exert a cardioprotective effect with distinct mechanisms of action, as evidenced by the differential kinetics of $\Delta\Psi_m$ loss; IPC may affect the latency period but not the depolarization period, and CsA may blunt the depolarization process but not affect the latency.

Study Limitations

Although this technique can be performed in whole tissue, the heart is not contracting at the time of observation, and hence, the mitochondrial response excludes the energetic demands of contractile function. Also, although TPLSM has allowed increased depth assessment, there is still room for improvement to assess the transmural mitochondrial response to ischemic and reperfusion stress.

Clinical Implications

In the present study, we have developed a real-time imaging system to monitor mitochondrial function in the perfused heart. Because mitochondria play important roles in cell death pathways, these organelles are potentially prime targets for therapeutic intervention.[6,30,31] The factors regulating the maintenance or disruption of mitochondrial function can be investigated in detail with this system. Mechanistic dissection of the sequence of events will pinpoint the therapeutic targets against ischemia/reperfusion injury. The effects of various candidate drugs can be tested with this system. Thus, this system will provide valuable information for a more integrated understanding of ischemia/reperfusion injury, and furthermore, it will provide deeper insights into the establishment of antiischemia/reperfusion therapy that targets mitochondria.

Acknowledgments

We thank Dr Steven P. Jones (University of Louisville) for his helpful comments and critical reading of the manuscript.

Sources of Funding

This work was supported by research grants (grants-in-aid in scientific research, leading project for biosimulation) from the Ministry of Education, Culture, Science, and Technology of Japan; a Japan Heart Foundation/Novartis grant for research award on molecular and cellular cardiology; and a research grant from Mitsubishi Pharma Research Foundation.

Disclosures

None.

References

1. Green DR, Kroemer G. The pathophysiology of mitochondrial cell death. *Science.* 2004;305:626–629.
2. Kroemer G, Reed JC. Mitochondrial control of cell death. *Nat Med.* 2000;6:513–519.
3. Halestrap AP, Clarke SJ, Javadov SA. Mitochondrial permeability transition pore opening during myocardial reperfusion: a target for cardioprotection. *Cardiovasc Res.* 2004;61:372–385.

Downloaded from circ.ahajournals.org at KYOTO UNIV Igaku Toshokan on April 3, 2007

4. Weiss JN, Korge P, Honda HM, Ping P. Role of the mitochondrial permeability transition in myocardial disease. *Circ Res.* 2003;93: 292–301.
5. Crompton M. The mitochondrial permeability transition pore and its role in cell death. *Biochem J.* 1999;341(pt 2):233–249.
6. Bouchier-Hayes L, Lartigue L, Newmeyer DD. Mitochondria: pharmacological manipulation of cell death. *J Clin Invest.* 2005;115:2640–2647.
7. Akao M, O'Rourke B, Teshima Y, Seharaseyon J, Marban E. Mechanistically distinct steps in the mitochondrial death pathway triggered by oxidative stress in cardiac myocytes. *Circ Res.* 2003;92:186–194.
8. Akao M, O'Rourke B, Kusuoka H, Teshima Y, Jones SP, Marban E. Differential actions of cardioprotective agents on the mitochondrial death pathway. *Circ Res.* 2003;92:195–202.
9. Aon MA, Cortassa S, O'Rourke B. Percolation and criticality in a mitochondrial network. *Proc Natl Acad Sci U S A.* 2004;101:4447–4452.
10. Murata M, Akao M, O'Rourke B, Marban E. Mitochondrial ATP-sensitive potassium channels attenuate matrix Ca^{2+} overload during simulated ischemia and reperfusion: possible mechanism of cardioprotection. *Circ Res.* 2001;89:891–898.
11. Levraut J, Iwase H, Shao ZH, Vanden Hoek TL, Schumacker PT. Cell death during ischemia: relationship to mitochondrial depolarization and ROS generation. *Am J Physiol Heart Circ Physiol.* 2003;284:H549–H558.
12. Bialik S, Cryns VL, Drincic A, Miyata S, Wollowick AL, Srinivasan A, Kitsis RN. The mitochondrial apoptotic pathway is activated by serum and glucose deprivation in cardiac myocytes. *Circ Res.* 1999;85: 403–414.
13. Denk W, Strickler JH, Webb WW. Two-photon laser scanning fluorescence microscopy. *Science.* 1990;248:73–76.
14. Rubart M. Two-photon microscopy of cells and tissue. *Circ Res.* 2004; 95:1154–1166.
15. Pacher P, Hajnoczky G. Propagation of the apoptotic signal by mitochondrial waves. *EMBO J.* 2001;20:4107–4121.
16. Halestrap AP, Connern CP, Griffiths EJ, Kerr PM. Cyclosporin A binding to mitochondrial cyclophilin inhibits the permeability transition pore and protects hearts from ischaemia/reperfusion injury. *Mol Cell Biochem.* 1997;174:167–172.
17. Murry CE, Jennings RB, Reimer KA. Preconditioning with ischemia: a delay of lethal cell injury in ischemic myocardium. *Circulation.* 1986; 74:1124–1136.
18. Dumont EA, Reutelingsperger CP, Smits JF, Daemen MJ, Doevendans PA, Wellens HJ, Hofstra L. Real-time imaging of apoptotic cell-membrane changes at the single-cell level in the beating murine heart. *Nat Med.* 2001;7:1352–1355.
19. Gottlieb RA, Kitsis RN. Seeing death in the living. *Nat Med.* 2001;7: 1277–1278.
20. Rubart M, Soonpaa MH, Nakajima H, Field LJ. Spontaneous and evoked intracellular calcium transients in donor-derived myocytes following intracardiac myoblast transplantation. *J Clin Invest.* 2004;114:775–783.
21. Rubart M, Pasumarthi KB, Nakajima H, Soonpaa MH, Nakajima HO, Field LJ. Physiological coupling of donor and host cardiomyocytes after cellular transplantation. *Circ Res.* 2003;92:1217–1224.
22. Petronilli V, Miotto G, Canton M, Brini M, Colonna R, Bernardi P, Di Lisa F. Transient and long-lasting openings of the mitochondrial permeability transition pore can be monitored directly in intact cells by changes in mitochondrial calcein fluorescence. *Biophys J.* 1999;76:725–734.
23. Molkentin JD. Calcineurin, mitochondrial membrane potential, and cardiomyocyte apoptosis. *Circ Res.* 2001;88:1220–1222.
24. Braunwald E, Kloner RA. Myocardial reperfusion: a double-edged sword? *J Clin Invest.* 1985;76:1713–1719.
25. Granville DJ, Tashakkor B, Takeuchi C, Gustafsson AB, Huang C, Sayen MR, Wentworth P Jr, Yeager M, Gottlieb RA. Reduction of ischemia and reperfusion-induced myocardial damage by cytochrome P450 inhibitors. *Proc Natl Acad Sci U S A.* 2004;101:1321–1326.
26. Akar FG, Aon MA, Tomaselli GF, O'Rourke B. The mitochondrial origin of postischemic arrhythmias. *J Clin Invest.* 2005;115:3527–3535.
27. Boban M, Stowe DF, Kampine JP, Goldberg AH, Bosnjak ZJ. Effects of 2,3-butanedione monoxime in isolated hearts: protection during reperfusion after global ischemia. *J Thorac Cardiovasc Surg.* 1993;105: 532–540.
28. Verrecchia F, Herve JC. Reversible blockade of gap junctional communication by 2,3-butanedione monoxime in rat cardiac myocytes. *Am J Physiol.* 1997;272:C875–C885.
29. Miura T, Ohnuma Y, Kuno A, Tanno M, Ichikawa Y, Nakamura Y, Yano T, Miki T, Sakamoto J, Shimamoto K. Protective role of gap junctions in preconditioning against myocardial infarction. *Am J Physiol Heart Circ Physiol.* 2004;286:H214–H221.
30. Murphy E. Primary and secondary signaling pathways in early preconditioning that converge on the mitochondria to produce cardioprotection. *Circ Res.* 2004;94:7–16.
31. O'Rourke B. Evidence for mitochondrial K^+ channels and their role in cardioprotection. *Circ Res.* 2004;94:420–432.

CLINICAL PERSPECTIVE

Mitochondria are crucial regulators of life and death in a variety of cells and play pivotal roles in cardiomyocyte death in response to myocardial ischemia/reperfusion. In the present study, for the first time, we successfully visualized mitochondrial function in living heart specimens and monitored the progressive changes of mitochondrial function in response to ischemia/reperfusion using 2-photon laser-scanning microscopy. Monitoring the spatiotemporal changes in mitochondrial function within single cardiomyocytes of an intact living heart would have tremendous advantages over the conventional in vitro models, because the heart is working as a syncytium in which individual cardiomyocytes are anatomically and functionally connected. Moreover, the pathological stimulus (ischemia/reperfusion) applied to the intact heart model is clinically relevant to ischemic heart disease in humans. Cardiac myocytes can undergo mitochondrial collapse during ischemia and can do so more prominently during reperfusion, which emphasizes the importance of reperfusion injury in the clinical setting. Ischemia/reperfusion results in marked cellular and subcellular heterogeneity in mitochondrial function, perhaps leading to electrical instability and arrhythmogenesis. Cardioprotective interventions (pharmacological or nonpharmacological) are now being applied in clinical medicine to reduce infarct size and improve the clinical status of patients with acute myocardial infarction. Thus, investigation of cellular responses in the natural environment will increase knowledge of ischemia/reperfusion injury and provide deeper insights into antiischemia/reperfusion therapy that targets mitochondria.

Downloaded from circ.ahajournals.org at KYOTO UNIV Igaku Toshokan on April 3, 2007

THE JOURNAL OF BIOLOGICAL CHEMISTRY VOL 281, NO 39, pp 28657–28665, September 29, 2006
© 2006 by The American Society for Biochemistry and Molecular Biology, Inc Printed in the U S A

Constitutive GDP/GTP Exchange and Secretion-dependent GTP Hydrolysis Activity for Rab27 in Platelets*

Received for publication, April 5, 2006, and in revised form, June 19, 2006 Published, JBC Papers in Press, July 31, 2006, DOI 10.1074/jbc.M603227200

Hirokazu Kondo[‡], Ryutaro Shirakawa[‡1], Tomohito Higashi[‡1], Mitsunori Kawato[‡], Mitsunori Fukuda[§¶], Toru Kita[‡], and Hisanori Horiuchi[‡2]

From the [‡]Department of Cardiovascular Medicine, Graduate School of Medicine, Kyoto University, Kyoto 606-8507, the [§]Fukuda Initiative Research Unit, RIKEN, Wako, Saitama 351-0198, and the [¶]Laboratory of Membrane Trafficking Mechanisms, Department of Developmental Biology and Neurosciences, Graduate School of Life Sciences, Tohoku University, Aobayama, Aoba-ku, Sendai, Miyagi 980-8578, Japan

We have previously demonstrated that Rab27 regulates dense granule secretion in platelets. Here, we analyzed the activation status of Rab27 using the thin layer chromatography method analyzing nucleotides bound to immunoprecipitated Rab27 and the pull-down method quantifying Rab27 bound to the GTP-Rab27-binding domain (synaptotagmin-like protein (Slp)-homology domain) of its specific effector, Slac2-b. We found that Rab27 was predominantly present in the GTP-bound form in unstimulated platelets due to constitutive GDP/GTP exchange activity. The GTP-bound Rab27 level drastically decreased due to enhanced GTP hydrolysis activity upon granule secretion. In permeabilized platelets, increase of Ca^{2+} concentration induced dense granule secretion with concomitant decrease of GTP-Rab27, whereas in non-hydrolyzable GTP analogue GppNHp (β-γ-imidoguanosine 5′-triphosphate)-loaded permeabilized platelets, the GTP (GppNHp)-Rab27 level did not decrease upon the Ca^{2+}-induced secretion. These data suggested that GTP hydrolysis of Rab27 was not necessary for inducing the secretion. Taken together, Rab27 is maintained in the active status in unstimulated platelets, which could function to keep dense granules in a preparative status for secretion.

In eukaryotic cells, transport between distinct organelles is performed through vesicle trafficking. The final step of vesicle docking/fusion with target membrane is mediated by *trans*-soluble *N*-ethylmaleimide-sensitive factor attachment protein receptor (SNARE)[3] complex bridging a vesicle and its target membrane (1). One of the key regulators for the SNARE complex formation is Rab GTPase (2, 3). So far, more than 60 members of Rab GTPases are identified in mammals, and they play critical roles in the specific transport pathways (2–4). Like other GTPases, the activity of Rab is regulated by its GDP/GTP cycle. Rab proteins have GTP-bound active and GDP-bound inactive forms. The activation process is performed by GDP/GTP exchange mediated by the GDP/GTP exchange factor. GTP-bound Rabs execute their function by interaction with effector proteins. Then, GTP-Rab is inactivated into GDP-Rab by GTP hydrolysis that is mediated by the intrinsic GTPase activity and its enhancer, GTPase-activating protein. Furthermore, the Rab family has a unique regulatory protein named Rab GDP dissociation inhibitor (RabGDI), which extracts GDP-Rab from membrane into cytosol by forming a 1:1 complex and inhibits GDP/GTP exchange (3). RabGDI accompanies Rabs in cytosol to the correct organelles, where they are reactivated by the function of GDI dissociation factor (5–8).

Although elucidation of the regulatory mechanism of the GDP/GTP cycle is crucial for understanding the functional mechanism of Rab GTPases, it has not been extensively investigated so far. Small GTPases belonging to Ras and Rho families are predominantly present in the GDP-bound forms under resting conditions and are transiently activated into GTP-bound forms upon stimulation (9), indicating that these GTPases function as "switches" that transduce extracellular signals. For Rab GTPases, most of Rab5, a regulator of endocytic pathway (10, 11), is in the GDP-bound form in unstimulated NR6 cells, and more than half of Rab5 rapidly and transiently becomes the GTP-bound active form upon epidermal growth factor stimulation (12). On the other hand, ~80% of Rab3D is in the GTP-bound form in unstimulated pancreatic acini (13). Since these two results are quite opposite, it is unclear whether RabGTPases are present in its GTP-bound or GDP-bound form. Furthermore, it is not known whether the activation status of other Rab GTPases is altered upon stimulation, like Rab5.

Rab27 is composed of two isoforms, Rab27A and Rab27B, that share ~70% identical amino acid residues (14–16). Accumulating evidence revealed that Rab27 is a general regulator for regulated exocytosis in non-neuronal cells, such as lytic granule

* This work was supported by Ministry of Education, Culture, Sports, Science, and Technology Research Grants, Japan, and by Health and Labor Sciences Research Grant for Cardiovascular Research from the Ministry of Health Labor and Welfare, Japan. This study was also supported in part by grants from the Takeda Science Foundation, Japan Heart Foundation Young Investigator's Research Grant and Japan Heart Foundation Pfizer Japan Inc. Grant for Research on Cardiovascular Disease. The costs of publication of this article were defrayed in part by the payment of page charges. This article must therefore be hereby marked "*advertisement*" in accordance with 18 U.S.C. Section 1734 solely to indicate this fact.

[1] Recipients of the Japan Society for the Promotion of Science Research Fellowship for Young Scientists.

[2] To whom correspondence should be addressed. Tel.: 81-75-751-3778; Fax: 81-75-751-3203; E-mail: horiuchi@kuhp.kyoto-u.ac.jp.

[3] The abbreviations used are: SNARE, soluble *N*-ethylmaleimide-sensitive factor attachment protein receptor; GDI, GDP dissociation inhibitor; Slp, synaptotagmin-like protein; SHD, synaptotagmin-like protein homology domain; Slac2, synaptotagmin-like protein homologue lacking C2 domains; GST, glutathione *S*-transferase; NEM, *N*-ethylmaleimide; GTPγS, guanosine 5′-3-*O*-(thio)triphosphate; GppNHp, β-γ-imidoguanosine 5′-triphosphate.

Downloaded from www.jbc.org at Kyoto University on April 3, 2007

secretion in cytotoxic T cells (17, 18), insulin secretion in pancreatic β-cells (19), and histamine-containing granule secretion in mast cells (20, 21). Rab27 also regulates melanosome traffic along actin cytoskeleton in melanocytes (22–25).

Dense granules in platelets contain self-agonists such as ADP and serotonin. Secreted ADP and serotonin play important roles for positive feedback activation of platelets at the site of thrombus formation (26, 27). We have demonstrated that Rab27 regulates the secretion in platelets by showing that the addition of non-prenylated Rab27A or Rab27B purified from *Escherichia coli* specifically inhibited the secretion in an assay using permeabilized platelets, possibly due to sequestering its putative effector molecules (28). We have identified a Rab27 effector in platelet cytosol as Munc13-4 (28). Munc13-4 is a non-neuronal homologue of Munc13-1, an essential priming factor in neuronal secretion.

In addition to Munc13-4, eight Rab27 effector molecules have been identified. Although a GTP-Rab27-binding minimal domain of Munc13-4 has not been determined, these eight molecules contain a common GTP-Rab27-binding structure named synaptotagmin-like protein (Slp)-homology domains (SHD) ~100 amino acid long at their N-terminal ends (16). These eight molecules are classified into two groups: Slp1~5 containing two C2 calcium-binding domains and Slp-lacking C2 domains (Slac2)-a~c (16). Although some SHDs potentially bind other Rab proteins in addition to Rab27, SHD of Slac2-b is specific for GTP-Rab27 among 20 tested Rab GTPases (16, 29).

Here, to analyze the GDP/GTP-bound status of Rab27 in platelets, we utilized two assays, a GTP-Rab27 pull-down assay using SHD of Slac2-b and an assay using thin layer chromatography analyzing GDP/GTP associated with immunoprecipitated Rab27. By these two methods, we demonstrated that Rab27 in unstimulated platelets was predominantly in the GTP-bound form, a state that was maintained by constitutive GDP/GTP exchange activity. The GTP-bound form of Rab27 drastically decreased upon granule secretion, due to enhanced GTP hydrolysis activity that was secretion-dependent. Furthermore, we showed that GTP hydrolysis of Rab27 might not be required for the induction of secretion in platelets, namely hydrolysis would be a consequence of secretion.

EXPERIMENTAL PROCEDURES

Materials—Rabbit polyclonal anti-Rab27A (28) and -Rab27B (30) antibodies were generated using His_6-Rab27A and glutathione *S*-transferase (GST)-Rab27B as antigens, respectively. For Rab27 immunoprecipitation, we used both antibodies in combination. Mouse monoclonal anti-His_6 antibody was purchased from Sigma. Horseradish peroxidase-labeled anti-rabbit and anti-mouse IgG polyclonal antibodies were from Amersham Biosciences and used as secondary antibodies for Western blot analysis visualized by the enhanced chemiluminescence method (Amersham Biosciences). Streptolysin-O was from Dr. S. Bhakdi (Mainz University, Mainz, Germany) (31). [α-^{32}P]GTP (3,000 Ci/mmol), and [γ-^{32}P]GTP (3,000 Ci/mmol) were purchased from PerkinElmer Life Sciences, and [^{32}P]phosphorus (200 μCi/mmol) was from Amersham Biosciences. Unless otherwise specified, all the other chemicals including nucleotides, *N*-ethylmaleimide (NEM), and thrombin were purchased from Sigma.

cDNA encoding rat Rab27A was kindly provided by Dr. Y. Nozawa (Gifu International Institute of Biotechnology, Gifu, Japan) (14). Human Rab27B cDNA was cloned from the Marathon-Ready human bone marrow cDNA (Clontech) by PCR. SHD of Slac2-b (KIAA0624) (amino acids 1–79) was generated by PCR using KIAA0624 clone provided by Kazusa DNA Research Institute as a template. All the sequences of PCR products were confirmed by a 3100 genetic analyzer (Applied Biosystems). cDNAs were subcloned into the prokaryotic expression vector pDEST17 (Invitrogen) for His_6-tagged protein and pGEX-2T (Amersham Biosciences) for GST fusion proteins. These His_6-tagged and GST fusion proteins were produced in *E. coli* strain BL21 and purified according to the manufacturers' instructions. All the purified recombinant proteins were extensively dialyzed against Buffer A (50 mM HEPES/KOH, pH 7.2, 78 mM KCl, 4 mM $MgCl_2$, 0.2 mM $CaCl_2$, 2 mM EGTA, 1 mM dithiothreitol) and stored at −80 °C until use. Protein concentrations were determined by the Bradford method (Bio-Rad) or from the intensities of the bands in Coomassie Blue-stained SDS-PAGE gels using bovine serum albumin as a standard.

Platelet Dense Granule Secretion Assays—Freshly obtained washed platelets (5×10^7 platelets/assay, counted with the Coulter counter) were incubated with [^{3}H]serotonin (Amersham Biosciences) to allow uptake into dense core granules (~20,000 cpm/assay) followed by washing with Buffer A. For the assay using intact platelets, they were stimulated with 0.5 units/ml thrombin (Sigma) at 30 °C for the indicated periods, and secreted [^{3}H]serotonin was measured by a liquid scintillation counter (Beckman) after removing platelets by centrifugation. The secretion levels of [^{3}H]serotonin were expressed as percentages of the total [^{3}H]serotonin in the platelets before the final incubation.

The method of dense granule secretion assay using platelets permeabilized by streptolysin-O was described previously (28, 32–35). Briefly, plasma membrane of [^{3}H]serotonin-loaded platelets was permeabilized with streptolysin-O in Buffer A, where the calculated free Ca^{2+} concentration was ~20 nM (36). The permeabilized platelets were incubated with ATP, human platelet cytosol at 2.0 mg of proteins/ml, and tested materials at 4 °C for 15–30 min followed by further incubation at 30 °C for 3 min. Finally, the platelets were stimulated with 20 μM Ca^{2+} (36) at 30 °C for the indicated periods, and the reaction was stopped by the addition of ice-cold Buffer A containing 10 mM EGTA.

Assay Analyzing Specific Binding of SHD of Slac2-b with GTP-Rab27—Binding of SHD of Slac2-b with Rab27 was performed by affinity chromatography. First, a non-hydrolyzable GTP analogue, GTPγS, and GDP-bound His_6-Rab27A and His_6-Rab27B were prepared by incubation of these GTPases (0.2 μM) with 1 mM GTPγS and GDP in the presence of 4 mM $MgCl_2$ and 10 mM EDTA at 30 °C for 30 min followed by the addition of 15 mM $MgCl_2$ to quit the reaction as described (7). Then, GDP- and GTPγS-preloaded Rab27 (1 μg) was incubated with glutathione-Sepharose beads (Amersham Biosciences) coated with GST-SHD of Slac2-b at 4 °C for 1 h in Buffer A and washed three times with the same buffer. Bead-

Downloaded from www.jbc.org at Kyoto University on April 3, 2007

associated His_6-Rab27 was analyzed by immunoblotting with anti-His_6 antibody.

GTP-Rab27 Pull-down Assay with GST-SHD of Slac2-b—The amount of GTP-bound Rab27 in platelets was measured by affinity pull-down using the SHD. The standard assay was as follows. Platelets isolated from freshly obtained whole blood were lysed in Buffer A containing 0.5% Triton X-100 and protease inhibitor mixture (P8340, Sigma) at 4 °C for 5 min followed by centrifugation at 300,000 × *g* for 5 min. This procedure completely extracted Rab27. Then, the supernatants were incubated with glutathione beads coated with 10 μg of GST-SHD at 4 °C for 30 min. The beads were washed three times with Buffer A containing 0.1% Triton X-100 and the protease inhibitor mixture, and bead-associated Rab27 was analyzed by immunoblotting with anti-Rab27 antibody. Densitometric analysis of appropriately exposed film was performed, and the signals were quantified using Image J 1.33u software (National Institutes of Health).

To calculate the ratio of GDP/GTP, the standards were produced as described previously (13). The same amount of aliquots of the Triton X-100 extract was incubated at 30 °C for 90 min in the presence of 10 mM EDTA and 4 mM $MgCl_2$ with 1 mM GppNHp (a non-hydrolyzable GTP analogue) or GDP followed by the addition of 15 mM $MgCl_2$ to quit the reaction and determination of GTP-bound Rab27 by the pull-down method. The amount of pulled down Rab27 in the platelet lysate after incubation with GppNHp was defined as 100%, and that with GDP was defined as 0%.

Evaluation of Nucleotide Bound to Rab27—Washed platelets (2×10^8 platelets/assay) were incubated with 300 μCi of [^{32}P]phosphorus (200 μCi/mmol; Amersham Biosciences) in Buffer B (138 mM NaCl, 2.9 mM KCl, 1.8 mM $CaCl_2$, 12 mM $NaHCO_3$, 0.49 mM $MgCl_2$, 5.5 mM glucose, 50 mM HEPES/KOH, pH 7.4) at 37 °C for 3 h. After the platelets were washed with Buffer B twice followed by incubation at 30 °C for 3 min, they were stimulated with 0.5 units/ml thrombin at 30 °C for 3 min. Then, platelets were lysed with Buffer A containing 0.5% Triton X-100 and the protease inhibitor mixture at 4 °C for 5 min. Supernatants after centrifugation were immunoprecipitated using anti-Rab27 antibodies at 4 °C for 30 min. Bound nucleotides were eluted in 25 μl of Buffer A containing 0.2% SDS, 10 mM EDTA, 1 mM GTP, and 1 mM GDP at 85 °C for 3 min. The samples (6 μl of each) were then spotted onto a polyethyleneimine-cellulose TLC plate (Merck) and developed for 90 min in 1 M $LiCl_2$ and 1 M formic acid. The plates were dried and placed at −80 °C for 36–48 h for autoradiography. Densitometric analysis of appropriately exposed film was performed, and the signals were quantified using Image J 1.33u software (National Institutes of Health).

Statistical Analysis—All values presented are means ± S.E. Student's *t* test was used in Fig. 7*A*. Values of $p < 0.05$ were considered statistically significant.

RESULTS

Characterization of the SHD of Slac2-b as the GTP-Rab27-interacting Domain—We first characterized the SHD of a Rab27-specific effector, Slac2-b. We examined whether GST-SHD specifically bound GTP-bound Rab27A and Rab27B, both

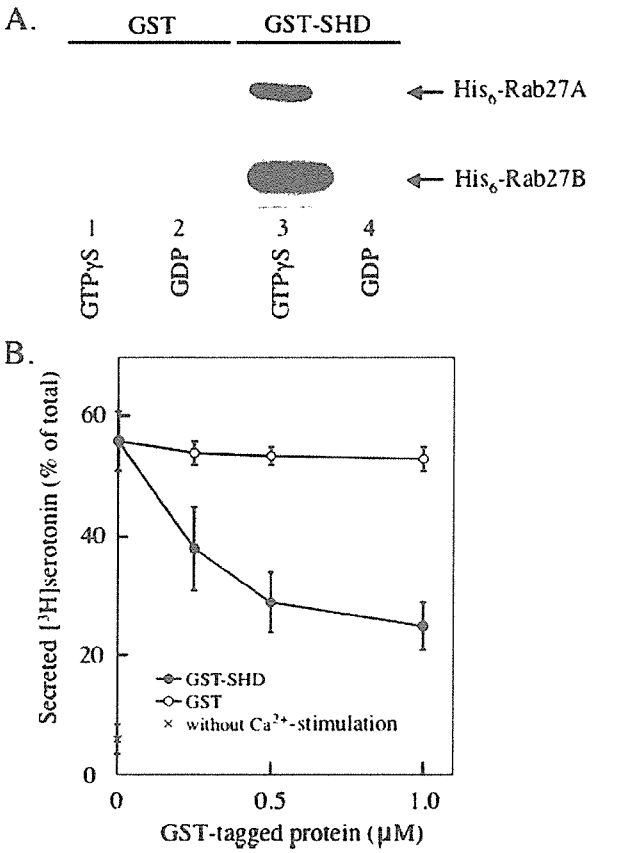

FIGURE 1. **Specific binding of SHD with GTP-Rab27 and its inhibitory effect on dense granule secretion in permeabilized platelets.** *A*, purified His_6-Rab27A (*upper panel*) and -Rab27B (*lower panel*) preloaded with GTPγS (*lanes 1* and *3*) or GDP (*lanes 2* and *4*) were incubated with glutathione beads coated with GST (*lanes 1* and *2*) and GST-SHD (*lanes 3* and *4*) at 4 °C for 1 h. After washing the beads, the bead-associated His_6-Rab27A and -Rab27B were detected by immunoblotting with anti-His_6 antibody as described under "Experimental Procedures." The data shown are representative of three independent experiments with similar results. *B*, permeabilized platelets were first incubated with various concentrations of GST (*open circles*) and GST-SHD (*closed circles*) at 4 °C for 30 min, and the Ca^{2+}-induced dense granule secretion ([^{3}H]serotonin) was analyzed as described under "Experimental Procedures." The secretion without the Ca^{2+} stimulation was shown (×). The results shown are expressed as means ± S.E. of three independent experiments.

of which are expressed in platelets (37). We incubated GTPγS (a non-hydrolyzable GTP analogue)-loaded and GDP-loaded His_6-Rab27 with GST-SHD-coated glutathione beads, and bead-associated Rab27 was analyzed by immunoblotting with anti-His_6 antibody. As shown in Fig. 1*A*, GST-SHD efficiently bound GTPγS-loaded Rab27A and Rab27B, with minimal binding to GDP-Rab27A and -Rab27B (Fig. 1*A*), indicating that the SHD specifically interacted with both GTP-Rab27A and GTP-Rab27B.

Next, we analyzed the involvement of Rab27 in the secretion using the SHD, which would sequester GTP-bound Rab27. In the assay, more than 50% of [^{3}H]serotonin preloaded into dense granules in permeabilized platelets was secreted within 1 min in response to Ca^{2+} stimulus at 30 °C, whereas the background secretion was 5–10% (Fig. 1*B*). The addition of GST-SHD, but not GST, in the assay efficiently inhibited the secretion in a concentration-dependent manner (Fig. 1*B*), supporting our

Downloaded from www.jbc.org at Kyoto University on April 3, 2007

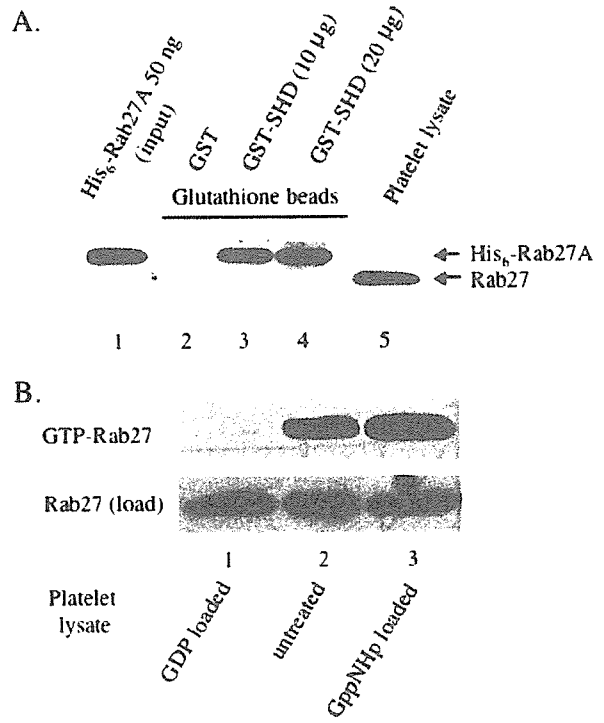

FIGURE 2. **A GTP-Rab27 pull-down assay using SHD revealed that GTP-Rab27 was predominant in unstimulated platelets.** *A*, GTP-loaded-His_6-Rab27A purified from *E. coli* (50 ng) (*lane 1*) was incubated at 4 °C for 30 min with glutathione beads coated with GST (*lane 2*), 10 μg of GST-SHD (*lane 3*), and 20 μg of GST-SHD (*lane 4*) followed by washing, and the bead-associated His_6-Rab27A was detected by immunoblotting with anti-Rab27 antibody as described under "Experimental Procedures." Platelet lysate isolated from 1 ml of blood was also analyzed (*lane 5*). The data shown are representative of three independent experiments with similar results. *B*, GTP-Rab27 in platelet lysate isolated from 1 ml of whole blood (*lane 2*) was incubated with glutathione beads coated with 10 μg of GST-SHD at 4 °C for 30 min, and bead-associated Rab27 was detected by immunoblotting with anti-Rab27 antibody as described under "Experimental Procedures." As controls, the same amounts of platelet lysates loaded *in vitro* with GDP (*lane 1*) or GppNHp (*lane 3*) were also analyzed in the same method. The data shown are representative of five independent experiments with similar results.

previous observation that Rab27 regulates dense granule secretion in platelets (28).

Establishment of GTP-Rab27 Pull-down Assay with SHD of Slac2-b—Most of Rab27 was present in the membrane fraction in platelets (34). To solubilize Rab27 from the membrane fraction in platelets, we used 0.5% Triton X-100, under which condition the interaction of the SHD with GTP-Rab27 was not affected. As shown in Fig. 2*A*, platelets ($\sim 5 \times 10^7$) isolated from 1 ml of blood contained ~50 ng of Rab27, determined using purified recombinant His_6-Rab27A as a reference. When the same amount (50 ng) of the recombinant His_6-Rab27A protein was used for a pull-down assay, almost all of the GTP-loaded form was bound to beads coated with 10 or 20 μg of GST-SHD but not to GST beads (Fig. 2*A*). Thus, this GST-SHD pull-down assay was established, and we used this method to evaluate the GTP-Rab27 levels in platelets.

Evaluation of GTP-Rab27 Level in Platelets—Using this pull-down assay, we evaluated the ratio of GTP-bound form of Rab27 in platelets. The results were calibrated as described previously (13), where the GDP/GTP-bound status of Rab3D in pancreatic acini was evaluated by their pull-down assay using a Rab3-effector RIM-1 (13). They solubilized pancreatic acinar cells, and the cell lysates were loaded with GTPγS or GDP. The amount of GST-RIM-1-associated Rab3D loaded with GTPγS was defined as 100%, and that loaded with GDP was defined as 0% (13). Here, we analyzed the GDP/GTP status of Rab27 in platelets and found that more than 70% (74.3 ± 3.0%, means ± S.E. of five individuals) of Rab27 was the GTP-bound form in unstimulated platelets (Fig. 2*B*).

We also evaluated the GDP/GTP-bound status of Rab27 by the thin layer chromatography method. Isolated platelets were first incubated at 37 °C for 3 h with [^{32}P]phosphorus that would be incorporated into GTP and GDP in platelets. As shown below (see Fig. 4*B*), nucleotide bound to immunoprecipitated Rab27 was predominantly GTP (62.7 ± 4.7%, means ± S.E. of three individuals). Thus, we obtained consistent results both by the pull-down and by the thin layer chromatography methods. We concluded that Rab27 was predominantly in the GTP-bound form in unstimulated platelets.

High Level of GTP-bound Rab27 Was Maintained by Constitutive GDP/GTP Exchange Activity in Platelets—We analyzed how the high level of GTP-Rab27 was maintained in unstimulated platelets. To examine this issue, permeabilized platelets were incubated in Buffer A (calculated free Ca^{2+} concentration was ~20 nM) (36) without the addition of ATP or platelet cytosol, where GTP would also be depleted by diffusion. In the platelets, the GTP-Rab27 level drastically decreased in a time-dependent manner measured by the Rab27 pull-down assay (Fig. 3, *A* and *C*), indicating that Rab27 in platelets was not fixed to be in the GTP-bound form. On the other hand, the same treatment of permeabilized platelets at 4 °C did not decrease GTP-Rab27 (Fig. 3*A*), indicating that this reaction is temperature-dependent. Importantly, this decrease was rescued by the addition of GTP in the system (Fig. 3, *B* and *C*), indicating that the high level of GTP-bound Rab27 was maintained most likely by GDP/GTP exchange reaction.

We examined whether the GDP/GTP exchange reaction indeed occurred in unstimulated platelets. We incubated permeabilized platelets with 10 μM [α-^{32}P]GTP at 30 °C in the absence of platelet cytosol. As shown in Fig. 3*D*, GTP-Rab27-associated radioactivity increased in a time-dependent manner, whereas amounts of GTP-Rab27 pulled down by the SHD were constant at any time point (data not shown), indicating that GDP/GTP exchange continuously took place to maintain the high level of GTP-Rab27 in unstimulated platelets. The rate of [α-^{32}P]GTP binding to endogenous Rab27 in permeabilized platelets was 0.032/min. Recombinant Rab27A protein purified from *E. coli in vitro* was examined in the same condition. The rate of [α-^{32}P]GTP binding to recombinant Rab27A was 0.0035/min (data not shown). Therefore, the GDP/GTP exchange rate for Rab27 in platelets was ~9 times faster than that of recombinant Rab27A. Since the exchange was so efficient in permeabilized platelets, in which the cytosol was extensively depleted due to diffusion, it is likely that the Rab27 GDP/GTP exchange factor, if any, is primarily membrane-associated.

GTP-bound Rab27 Decreased upon Granule Secretion through Enhanced GTP Hydrolysis Activity—We next examined the effect of granule secretion induced by an agonist on the

Downloaded from www.jbc.org at Kyoto University on April 3, 2007

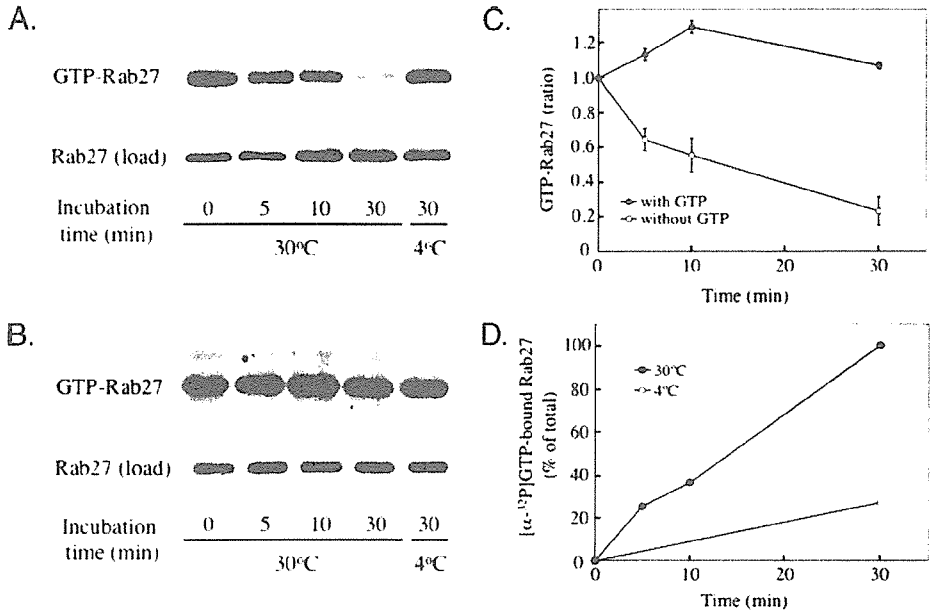

FIGURE 3. **Time-dependent decrease of GTP-Rab27 in permeabilized platelets, which was rescued by addition of GTP.** *A and B*, permeabilized platelets were incubated without the exogenous addition of ATP or platelet cytosol for the indicated periods at 30 °C or 4 °C, in the absence (*A*) or presence (*B*) of 1 mM GTP. GTP-Rab27 (*upper panels*) was measured by the GTP-Rab27 pull-down assay as described under "Experimental Procedures." The total Rab27 in the samples was shown in the *lower panels*. The data shown are representative of three independent experiments with similar results. *C*, time-dependent relative changes of GTP-Rab27 shown in *A* and *B* were presented using the GTP-Rab27 ratio at time 0 as a standard (1.0). The results shown are expressed as means ± S.E. of three independent experiments. *D*, permeabilized platelets were incubated with [α-^{32}P]GTP at 10 μM (10,000 cpm/pmol) for the indicated periods at 30 °C or 4 °C, and then GTP-Rab27 was pulled down by GST-SHD beads followed by quantification of [α-^{32}P]GTP as described under "Experimental Procedures." The results shown are representative of two independent experiments with similar results.

GDP/GTP status of Rab27. Upon 0.5 units/ml thrombin stimulation at 30 °C, GTP-Rab27 decreased from 74.3 ± 3.0 to 27.1 ± 6.3% at 3 min in intact platelets quantified by the pull-down assay (Fig. 4*A*). Similar results were obtained by the thin layer chromatography (Fig. 4*B*). After the thrombin stimulation for 3 min, GTP-Rab27 decreased from 62.7 ± 4.7 to 31.4 ± 1.4%, whereas GDP-Rab27 increased from 37.3 ± 4.7 to 68.6 ± 1.4%. Thus, Rab27-bound GTP drastically decreased with concomitant increase of Rab27-bound GDP upon stimulation, indicating that GTP hydrolysis of Rab27 was enhanced upon stimulation. The rate of GTP hydrolysis on Rab27 in thrombin-stimulated intact platelets in the thin layer chromatography method was 0.104/min. The rate of [γ-^{32}P]GTP hydrolysis on recombinant Rab27A purified from *E. coli* was 0.0056/min (data not shown). Therefore, the GTP hydrolysis velocity on Rab27 in stimulated platelets was ~18 times faster than that of recombinant Rab27A.

Decrease of GTP-Rab27 was also observed in permeabilized platelets undergoing the Ca^{2+}-induced granule secretion (Fig. 5*A*), and the degree of decrease was similar to that in thrombin-stimulated intact platelets (Fig. 4*A*). To examine whether GDP/GTP exchange activity was altered during the Ca^{2+}-induced granule secretion, permeabilized platelets were first incubated with [α-^{32}P]GTP, which would be loaded to small GTPases including Rab27 followed by the addition of excess non-labeled GTP. These platelets were incubated with ATP and platelet cytosol with or without Ca^{2+} stimulation. Then, time-dependent change of [α-^{32}P]GTP-Rab27 was compared. As shown in Fig. 5*B*, [α-^{32}P]GTP levels associated with immunoprecipitated Rab27 decreased over time similarly with or without Ca^{2+} stimulation. Since [α-^{32}P]GTP level associated with immunoprecipitated Rab27 would be affected by GDP/GTP exchange but not GTP hydrolysis, these results indicated that the GDP/GTP exchange activity was not affected upon stimulation.

Granule secretion is triggered by elevation of Ca^{2+} concentration (38). Since calcium ions regulate many cellular functions, we tried to address which triggered the decrease of GTP-Rab27, elevated Ca^{2+} concentration or secretion itself. We addressed this issue by using NEM, which is an inhibitor of an essential regulator of the SNARE system, NEM-sensitive factor. NEM inhibited the Ca^{2+}-induced dense granule secretion in a concentration-dependent manner in permeabilized platelets (Fig. 6*A*) as shown previously (39). Under these conditions, NEM treatment inhibited the decrease of the GTP-Rab27 level, although permeabilized platelets were stimulated with high concentration of Ca^{2+} (Fig. 6*B*). These data indicated that the fusion of the granules with plasma membrane, rather than the elevation of Ca^{2+} concentration, is required for enhancement of Rab27-associated GTP hydrolysis.

GTP Hydrolysis of Rab27 Did Not Appear Essential for the Dense Granule Secretion—To find out the implication of the high level of GTP-bound Rab27 and its secretion-dependent GTP hydrolysis, we tried to address whether GTP hydrolysis was required for granule secretion. It is well known that non-hydrolyzable GTP analogue at 100 μM promotes the Ca^{2+}-independent granule secretion in permeabilized platelets (40). However, in permeabilized platelets preincubated with a lower concentration of GppNHp at 10 μM, we observed a significant increase of the granule secretion upon Ca^{2+} stimulation (in Fig. 7*A*, compare *lane 4* and *lane 5*)($p < 0.01$), although the secretion level without Ca^{2+} stimulation was rather high (Fig. 7*A*, *lane 4*). Importantly, the Ca^{2+}-dependent secretion was reduced by the addition of the SHD (Fig. 7*A*, compare *lane 5* and *lane 6*)($p < 0.05$), indicating that Rab27 was involved in this secretion. Under this condition, in contrast to GTP-bound Rab27 (Fig. 7*B*, *lanes 1–3*), the GppNHp-bound form of Rab27 did not decrease upon granule secretion measured by the pull-down assay, indicating that the majority of Rab27 remained bound to GppNHp in the permeabilized platelets (Fig. 7*B*, *lanes 4–6*). Taken together, GTP hydrolysis of Rab27 did not appear necessary for the induction of granule secretion in platelets.

Downloaded from www.jbc.org at Kyoto University on April 3, 2007

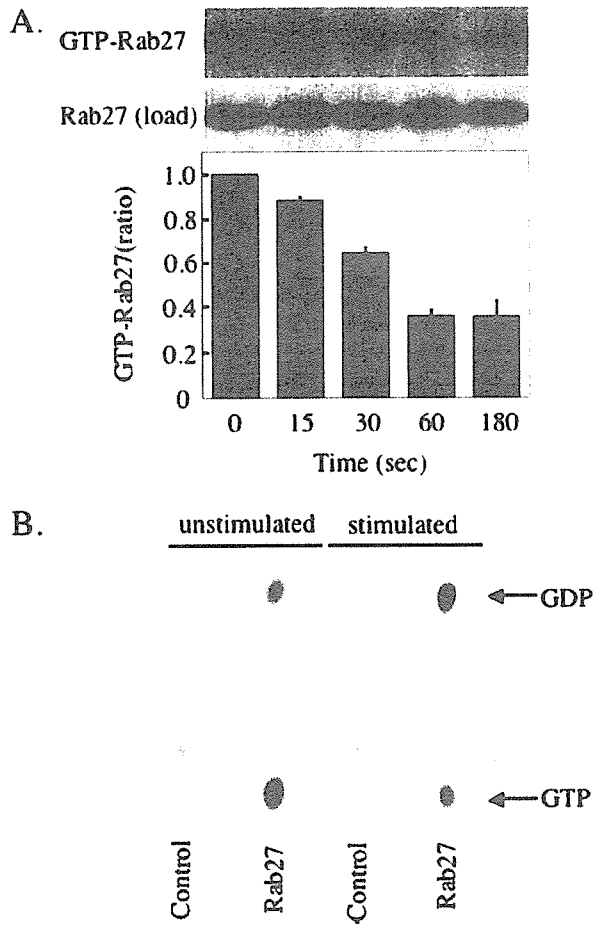

FIGURE 4. **GTP-Rab27 decreased upon granule secretion through enhanced GTP hydrolysis activity.** *A*, isolated platelets were stimulated with 0.5 units/ml thrombin for the indicated periods at 30 °C. Then, GTP-Rab27 (*upper panel*) was measured by the GTP-Rab27 pull-down assay as described under "Experimental Procedures." The total Rab27 in the samples was shown in the *lower panel*. Relative changes of GTP-Rab27 were presented using the GTP-Rab27 ratio at time 0 as a standard (1.0). The data shown are expressed as means ± S.E. of three independent experiments. *B*, isolated platelets were labeled with [^{32}P]phosphorus and then stimulated with 0.5 units/ml thrombin at 30 °C for 3 min. Rab27 was immunoprecipitated, and the bound nucleotides were analyzed by thin layer chromatography as described under "Experimental Procedures." The results shown are representative of three independent experiments with similar results.

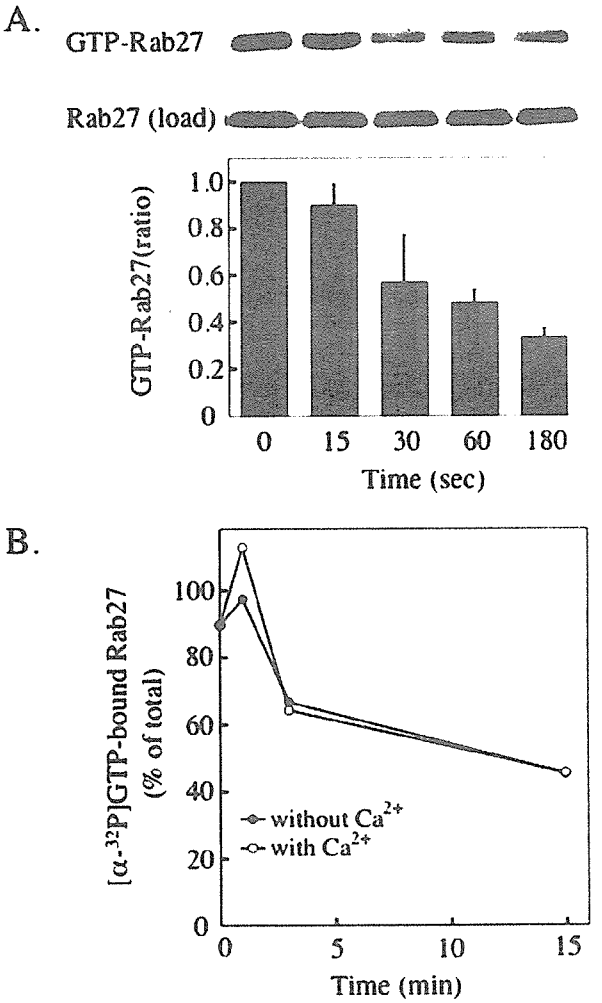

FIGURE 5. **The decrease of the GTP-Rab27 ratios upon the Ca^{2+}-induced secretion was not dependent on alteration of GDP/GTP exchange activity.** *A*, permeabilized platelets were stimulated in the presence of platelet cytosol and ATP by 20 μM Ca^{2+} for the indicated periods at 30 °C, and GTP-Rab27 (*upper panel*) was measured by the GTP-Rab27 pull-down assay as described under "Experimental Procedures." The total Rab27 in the samples was shown in the *lower panel*. Relative changes of GTP-Rab27 were presented using the GTP-Rab27 ratio at time 0 as a standard (1.0). The data shown are expressed as means ± S.E. of three independent experiments. *B*, permeabilized platelets were incubated with 10 μM [α-^{32}P]GTP at 30 °C for 30 min followed by the addition of cold excess GTP at 1 mM. These platelets were then incubated with or without 20 μM Ca^{2+} at 30 °C for the indicated periods, and the radioactivity associated with immunoprecipitated Rab27 was measured as described under "Experimental Procedures." The results shown are representative of two independent experiments with similar results.

DISCUSSION

In this study, we have analyzed the GDP/GTP cycle of endogenous Rab27 in platelets during regulated exocytosis and demonstrated that Rab27 was predominantly present in the GTP-bound form in unstimulated platelets and GTP-bound Rab27 decreased upon granule secretion. The activation status of Rab27 was regulated by constitutive GDP/GTP exchange activity and secretion-dependent GTP hydrolysis activity. Furthermore, we showed that GTP hydrolysis of Rab27 would not be essential for inducing the secretion. With these experimental results, we propose that the function of Rab27 in the platelet secretion is to maintain the granules in a preparative status for the secretion rather than to mediate the secretion signal.

We have established two methods for quantifying GTP-Rab27. One is the pull-down method in which we use the GTP-Rab27-binding domain, SHD, of a Rab27-specific effector molecule, Slac2-b (29). Since this SHD specifically interacted with GTP-Rab27 (Fig. 1*A*) and the interaction was unaffected by the detergent to solubilize Rab27, we could obtain reproducible results by this method. Another method is the thin layer chromatography method in which radioactive nucleotide bound to immunoprecipitated Rab27 was analyzed. The results obtained by these two independent methods were coincided. In contrast to the thin layer chromatography, which utilizes high levels of radioactivity and much primary antibodies, the pull-down assay is a preferred method to obtain equivalent results. Therefore, most of the experiments were performed with the pull-down assay, and key experiments for critical confirmation were performed with both methods.

The Journal of Biological Chemistry 2006

Downloaded from www.jbc.org at Kyoto University on April 3, 2007

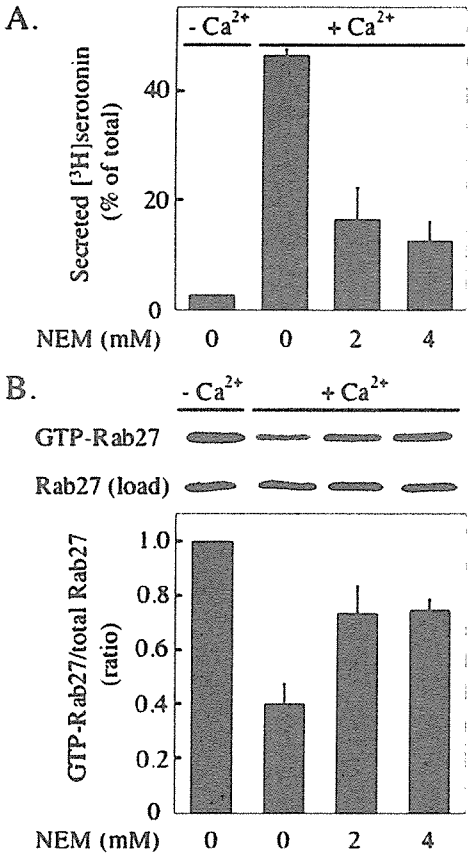

FIGURE 6. **The Ca^{2+} stimulation did not induce the decrease of GTP-Rab27 ratios when the secretion was inhibited by NEM in permeabilized platelets.** *A*, permeabilized platelets were incubated in the presence of platelet cytosol and ATP with various concentration of NEM at 4 °C for 30 min followed by the Ca^{2+} stimulation at 30 °C for 1 min. The Ca^{2+}-induced dense granule secretion was analyzed as described under "Experimental Procedures." The data shown are expressed as means ± S.E. of three independent experiments. *B*, GTP-Rab27 (*upper panel*) in these platelets was measured by the GTP-Rab27 pull-down assay as described under "Experimental Procedures." The total Rab27 in the samples was shown in the *lower panel*. Relative changes of GTP-Rab27 were presented using the GTP-Rab27 ratio at time 0 as a standard (1.0). The data shown are expressed as means ± S.E. of three independent experiments.

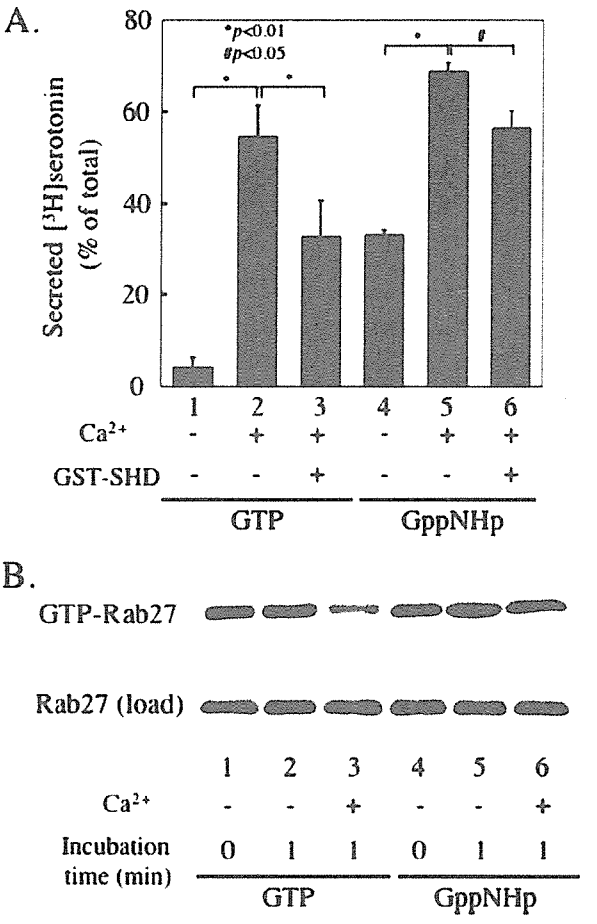

FIGURE 7. **GTP hydrolysis of Rab27 did not appear essential for the dense granule secretion.** *A*, permeabilized platelets were incubated with 10 μM GTP (*lanes 1–3*) or GppNHp (*lanes 4–6*) in the absence of platelet cytosol and ATP at 30 °C for 15 min followed by the addition of platelet cytosol and ATP. These permeabilized platelets were incubated with (*lanes 3* and *6*) or without (*lanes 1, 2, 4,* and *5*) 1 μM GST-SHD at 4 °C for 15 min. These permeabilized platelets were incubated with or without Ca^{2+} for 1 min, and secreted [^{3}H]serotonin was analyzed as described under "Experimental Procedures." The results shown are expressed as means ± S.E. of five independent experiments. *, $p < 0.01$, *lane 1 versus lane 2*, *lane 2 versus lane 3*, and *lane 4 versus lane 5*. #, $p < 0.05$, *lane 5 versus lane 6*. *B*, GTP- (or GppNHp-) Rab27 (*upper panel*) in these platelets was measured by the GTP-Rab27 pull-down assay as described under "Experimental Procedures." The total Rab27 in the samples was shown in the *lower panel*. The results shown are representative of three independent experiments with similar results.

We investigated the mechanism by which GTP-Rab27 is maintained at such a high level. Two possibilities were conceivable; GTP bound to Rab27 is statically kept without entering the GDP/GTP cycle, or the GTP-bound form is maintained in a dynamic equilibrium between GTP hydrolysis and GDP/GTP exchange activities. Here, the data demonstrated the high rates of nucleotide exchange for Rab27 in unstimulated platelets. First, GTP-Rab27 levels decreased in permeabilized platelets without the addition of GTP in the milieu. Second, this decrease was rescued by the addition of GTP in the system. Third, [α-^{32}P]GTP added in the system was incorporated to Rab27 in a time-dependent manner, whereas total GTP-Rab27 levels were not changed. Thus, the high level of GTP-bound Rab27 in unstimulated platelets was maintained by constitutive GDP/GTP exchange activity. Since we detected GDP/GTP exchange activity for Rab27 in permeabilized platelets, where the cytosol was extensively depleted, the majority of the GDP/GTP exchange activity could be membrane-associated.

Rybin *et al.* (41) have examined the GDP/GTP cycle of Rab5 on purified early endosomal membrane in the steady states by experiments analyzing xanthosine 5′-triphosphate bound to mutant Rab5, which preferentially binds xanthosine 5′-triphosphate instead of GTP. They demonstrated that Rab5 activity is regulated in a dynamic equilibrium by constitutive GTP hydrolysis activity on purified early endosome membrane. Then, they speculated that Rab5 undergoes multiple cycles of nucleotide binding and hydrolysis on the early endosome membrane (41).

Since GDP-bound Rab GTPases could be present in cytosol by forming a complex with RabGDI, the data that most of Rab27 localizes in the membrane fraction (33) could reflect the predominant existence of Rab27 in the GTP-bound form in platelets. Since GDP/GTP exchange occurred in Rab27 in permeabilized platelets without the addition of platelet cytosol containing RabGDI (Fig. 3, *A*, *B*, and *D*), Rab27 appears to undergo multiple GDP/GTP cycle on the membrane, similar to Rab5, without recycling between cytosol and membrane.

Downloaded from www.jbc.org at Kyoto University on April 3, 2007

Here, we demonstrated that the high level of GTP-Rab27 markedly decreased upon stimulation in platelets due to enhanced Rab27 GTP hydrolysis activity. Since the GDP/GTP exchange activity for Rab27 appeared unchanged by granule secretion (Fig. 5*B*), this decrease of GTP-Rab27 would be exclusively due to the enhanced GTP hydrolysis activity upon stimulation. The granule secretion is triggered by increased Ca^{2+} concentration. However, the Rab27 GTP hydrolysis activity was not enhanced by increased Ca^{2+} concentration alone. It was coupled with granule secretion *per se* since increased Ca^{2+} concentration did not decrease the GTP-Rab27 level when the secretion was inhibited by NEM.

What is the implication of the high active status of Rab27 in unstimulated platelets and GTP hydrolysis upon granule secretion? If GTP hydrolysis of Rab27 is not required for the secretion, the predominant presence of Rab27 in its active form would imply that Rab27 does not mediate the secretion signal directly but rather plays a role to maintain the vesicles in the preparative state for secretion. If GTP hydrolysis of Rab27 is required for fusion, GTP-Rab27 would function as a negative regulator, where the secretion signal induces GTP hydrolysis of Rab27 to trigger the secretion. To date, two types of functional mechanisms of GTPases are known. Some require GTP hydrolysis for the function, and the others do not require it. For examples, elongation factor EF-Tu requires GTP hydrolysis to perform the proofreading of elongation of the correct amino acid at the end of peptide under production (42). On the other hand, the GTP-bound form of Rab5 is the active form, which induces membrane docking/fusion of early endosomes without requiring GTP hydrolysis (11, 41). Therefore, elucidation of the implication of GTP hydrolysis of Rab27 is essential to understand the functional mechanism of Rab27 in the regulation of the secretion.

To address this issue, we used non-hydrolyzable GTP analogue, GppNHp, in the assay system with permeabilized platelets. It is well known that non-hydrolyzable GTP analogue at 100 μM promotes the Ca^{2+}-independent granule secretion in permeabilized platelets (40). However, in permeabilized platelets preincubated with a lower concentration of GppNHp at 10 μM, we observed a significant increase of the granule secretion upon Ca^{2+} stimulation. In this experiment, the GTP-Rab27 level did not decrease by the granule secretion, suggesting that almost all Rab27 bound GppNHp. Furthermore, the Ca^{2+}-induced secretion in the presence of 10 μM GppNHp was inhibited by the addition of the GTP-Rab27-binding domain, SHD (Fig. 7*A*, *lane 6*), indicating that Rab27 played a role for inducing the secretion. Therefore, we would conclude that GTP-Rab27 is the active form and GTP hydrolysis of Rab27 does not appear necessary for dense granule secretion in platelets.

Since Rab27 in platelets is predominantly present in its GTP-bound form and GTP hydrolysis appears unnecessary for the secretion, it is likely that GTP-Rab27 would not mediate extracellular signals but rather keep the vesicles in a preparative state for the secretion. Since increased Ca^{2+} concentration is the trigger of the secretion (38), the calcium ion signal would be mediated by a calcium-binding protein such as a Rab27 effector molecule Munc13-4 containing Ca^{2+}-binding C2 domains (28), and protein kinase C (33).

Nevertheless, we cannot completely exclude the possibility that GTP hydrolysis of Rab27 is required for the granule secretion due to some limitations in the experiments shown in Fig. 7 to address the requirement of GTP hydrolysis of Rab27 for the secretion. First, other GTPases as well as Rab27 would bind GppNHp in permeabilized platelets. Some of these GTPases might bypass the need for GTP hydrolysis of Rab27. Second, the spans of the Ca^{2+}-induced secretion and the inhibition by the SHD were relatively small in the assay due to rather high levels of secretion without Ca^{2+} stimulation in the presence of GppNHp. Although the differences are statistically significant, additional experiments would be required for the definite conclusion.

At this time, the biological implication of the secretion-dependent GTP hydrolysis of Rab27 remains unclear. It might play a role in recycling of Rab27 from the plasma membrane after one cycle of the secretion is completed.

Platelets contain many small GTPases, such as Ras, RhoA, Rap1, and Ral, that are predominantly present in their GDP-bound forms and transiently become GTP-bound forms upon stimulation in platelets (43–46). In contrast to these small GTPases, the GDP/GTP cycle of Rab27 appears unique. Given that Rab27 in platelets was predominantly in the GTP-bound form, the GDP/GTP exchange activity would be more dominant than the GTP hydrolysis activity in unstimulated platelets. Furthermore, this GDP/GTP exchange activity for Rab27 was not changed by the elevation of Ca^{2+} concentration (Fig. 5*B*), unlike that for other small GTPases (12, 46). Very recently, the GDP/GTP cycle of Arf6 has been demonstrated to be similar to that of Rab27 (46), where most of Arf6 is present in its GTP-bound form and GTP-Arf6 is decreased by agonist stimulation to regulate Rho family GTPases in platelets, although it has not been addressed whether GTP hydrolysis plays a role or not in its functions (46).

In pancreatic acini, most of Rab3D has been demonstrated to be in the GTP-bound form (13), although the GDP/GTP status of Rab3D in response to cellular stimulus has not been addressed. Since the Rab3 family is implicated in regulated exocytosis and related to Rab27 in the primary structure (16), the predominant GTP-bound form in the resting cells might be common in Rab GTPases implicated in regulated exocytosis.

Here, we showed that Rab27 in unstimulated platelets was predominantly present in the GTP-bound active form, which was regulated by its constitutive GDP/GTP exchange activity in a dynamic equilibrium and that this high level of GTP-Rab27 drastically decreased upon granule secretion due to enhanced GTP hydrolysis activity. To elucidate the molecular mechanism of the regulation in the secretion, it would be crucial to identify GTPase-activating protein and GDP/GTP exchange factor for Rab27 in platelets and characterize their functions in the platelet secretion.

Acknowledgments—We are grateful to Dr. Yoshinori Nozawa for providing a plasmid containing Rab27A and to Kazusa DNA Research Institute for providing KIAA0624. We are also grateful to the Kyoto Red Cross Blood Center for providing platelet pellets. We thank Dr. Heidi McBride (Ottawa) and Dr. Yasuyuki Fujita (London) for critical reading of the manuscript and Tomoko Matsubara for excellent technical assistance.

The Journal of Biological Chemistry

Downloaded from www.jbc.org at Kyoto University on April 3, 2007

REFERENCES

1. Chen, Y. A., and Scheller, R. H. (2001) *Nat. Rev. Mol. Cell. Biol.* **2,** 98–106
2. Zerial, M., and McBride, H. (2001) *Nat. Rev. Mol. Cell. Biol.* **2,** 107–117
3. Takai, Y., Sasaki, T., and Matozaki, T. (2001) *Physiol. Rev.* **81,** 153–208
4. Jordens, I., Marsman, M., Kuijl, C., and Neefjes, J. (2005) *Traffic* **6,** 1070–1077
5. Ullrich, O., Horiuchi, H., Bucci, C., and Zerial, M. (1994) *Nature* **368,** 157–160
6. Soldati, T., Shapiro, A. D., Svejstrup, A. B., and Pfeffer, S. R. (1994) *Nature* **369,** 76–78
7. Horiuchi, H., Giner, A., Hoflack, B., and Zerial, M. (1995) *J. Biol. Chem.* **270,** 11257–11262
8. Dirac-Svejstrup, A. B., Sumizawa, T., and Pfeffer, S. R. (1997) *EMBO J.* **16,** 465–472
9. Satoh, T., Endo, M., Nakafuku, M., Akiyama, T., Yamamoto, T., and Kaziro, Y. (1990) *Proc. Natl. Acad. Sci. U. S. A.* **87,** 7926–7929
10. Bucci, C., Parton, R. G., Mather, I. H., Stunnenberg, H., Simons, K., Hoflack, B., and Zerial, M. (1992) *Cell* **70,** 715–728
11. Stenmark, H., Parton, R. G., Steele-Mortimer, O., Lutcke, A., Gruenberg, J., and Zerial, M. (1994) *EMBO J.* **13,** 1287–1296
12. Barbieri, M. A., Roberts, R. L., Gumusboga, A., Highfield, H., Alvarez-Dominguez, C., Wells, A., and Stahl, P. D. (2000) *J. Cell Biol.* **151,** 539–550
13. Chen, X., Ernst, S. A., and Williams, J. A. (2003) *J. Biol. Chem.* **278,** 50053–50060
14. Nagata, K., Satoh, T., Itoh, H., Kozasa, T., Okano, Y., Doi, T., Kaziro, Y., and Nozawa, Y. (1990) *FEBS Lett.* **275,** 29–32
15. Chen, D., Guo, J., Miki, T., Tachibana, M., and Gahl, W. A. (1997) *Biochem. Mol. Med.* **60,** 27–37
16. Fukuda, M. (2005) *J. Biochem. (Tokyo)* **137,** 9–16
17. Stinchcombe, J. C., Barral, D. C., Mules, E. H., Booth, S., Hume, A. N., Machesky, L. M., Seabra, M. C., and Griffiths, G. M. (2001) *J. Cell Biol.* **152,** 825–834
18. Haddad, E. K., Wu, X., Hammer, J. A., III, and Henkart, P. A. (2001) *J. Cell Biol.* **152,** 835–842
19. Yi, Z., Yokota, H., Torii, S., Aoki, T., Hosaka, M., Zhao, S., Takata, K., Takeuchi, T., and Izumi, T. (2002) *Mol. Cell. Biol.* **22,** 1858–1867
20. Neeft, M., Wieffer, M., de Jong, A. S., Negroiu, G., Metz, C. H., van Loon, A., Griffith, J., Krijgsveld, J., Wulffraat, N., Koch, H., Heck, A. J., Brose, N., Kleijmeer, M., and van der Sluijs, P. (2005) *Mol. Biol. Cell* **16,** 731–741
21. Goishi, K., Mizuno, K., Nakanishi, H., and Sasaki, T. (2004) *Biochem. Biophys. Res. Commun.* **324,** 294–301
22. Wu, X. S., Rao, K., Zhang, H., Wang, F., Sellers, J. R., Matesic, L. E., Copeland, N. G., Jenkins, N. A., and Hammer, J. A., III (2002) *Nat. Cell Biol.* **4,** 271–278
23. Hume, A. N., Collinson, L. M., Rapak, A., Gomes, A. Q., Hopkins, C. R., and Seabra, M. C. (2001) *J. Cell Biol.* **152,** 795–808
24. Fukuda, M., Kuroda, T. S., and Mikoshiba, K. (2002) *J. Biol. Chem.* **277,** 12432–12436
25. Nagashima, K., Torii, S., Yi, Z., Igarashi, M., Okamoto, K., Takeuchi, T., and Izumi, T. (2002) *FEBS Lett.* **517,** 233–238
26. Brass, L. F. (2005) in *Hematology: The Molecular Basis of Platelet Activation* (Hoffman, R., Benz, E. J., Jr., Shattil, S. J., Furie, B., Cohen, H. J., Silberstein, L. E., and McGlave, P. eds) 4th Ed., pp. 1889–1914, Elsevier, NY
27. Horiuchi, H. (2006) *Ann. Med.* **38,** 162–172
28. Shirakawa, R., Higashi, T., Tabuchi, A., Yoshioka, A., Nishioka, H., Fukuda, M., Kita, T., and Horiuchi, H. (2004) *J. Biol. Chem.* **279,** 10730–10737
29. Kuroda, T. S., Fukuda, M., Ariga, H., and Mikoshiba, K. (2002) *J. Biol. Chem.* **277,** 9212–9218
30. Imai, A., Yoshie, S., Nashida, T., Shimomura, H., and Fukuda, M. (2004) *J. Cell Sci.* **117,** 1945–1953
31. Bhakdi, S., Weller, U., Walev, I., Martin, E., Jonas, D., and Palmer, M. (1993) *Med. Microbiol. Immunol. (Berl.)* **182,** 167–175
32. Yoshioka, A., Horiuchi, H., Shirakawa, R., Nishioka, H., Tabuchi, A., Higashi, T., Yamamoto, A., and Kita, T. (2001) *Ann. N. Y. Acad. Sci.* **947,** 403–406
33. Yoshioka, A., Shirakawa, R., Nishioka, H., Tabuchi, A., Higashi, T., Ozaki, H., Yamamoto, A., Kita, T., and Horiuchi, H. (2001) *J. Biol. Chem.* **276,** 39379–39385
34. Shirakawa, R., Yoshioka, A., Horiuchi, H., Nishioka, H., Tabuchi, A., and Kita, T. (2000) *J. Biol. Chem.* **275,** 33844–33849
35. Shirakawa, R., Higashi, T., Kondo, H., Yoshioka, A., Kita, T., and Horiuchi, H. (2005) *Methods Enzymol.* **403,** 778–788
36. Fabiato, A., and Fabiato, F. (1979) *J. Physiol. (Paris)* **75,** 463–505
37. Barral, D. C., Ramalho, J. S., Anders, R., Hume, A. N., Knapton, H. J., Tolmachova, T., Collinson, L. M., Goulding, D., Authi, K. S., and Seabra, M. C. (2002) *J. Clin. Investig.* **110,** 247–257
38. Knight, D. E., Hallam, T. J., and Scrutton, M. C. (1982) *Nature* **296,** 256–257
39. Polgar, J., and Reed, G. L. (1999) *Blood* **94,** 1313–1318
40. Coorssen, J. R., and Haslam, R. J. (1993) *FEBS Lett.* **316,** 170–174
41. Rybin, V., Ullrich, O., Rubino, M., Alexandrov, K., Simon, I., Seabra, M. C., Goody, R., and Zerial, M. (1996) *Nature* **383,** 266–269
42. Bourne, H. R. (1988) *Cell* **53,** 669–671
43. Franke, B., Akkerman, J. W., and Bos, J. L. (1997) *EMBO J.* **16,** 252–259
44. Bodie, S. L., Ford, I., Greaves, M., and Nixon, G. F. (2001) *Biochem. Biophys. Res. Commun.* **287,** 71–76
45. Wolthuis, R. M., Franke, B., van Triest, M., Bauer, B., Cool, R. H., Camonis, J. H., Akkerman, J. W., and Bos, J. L. (1998) *Mol. Cell. Biol.* **18,** 2486–2491
46. Choi, W., Karim, Z. A., and Whiteheart, S. W. (2006) *Blood* **107,** 3145–3152

Downloaded from www.jbc.org at Kyoto University on April 3, 2007

ATH-9759; No. of Pages 9

ELSEVIER

Atherosclerosis xxx (2007) xxx–xxx

ATHEROSCLEROSIS

www.elsevier.com/locate/atherosclerosis

Lectin-like oxidized LDL receptor-1 (LOX-1) expression is associated with atherosclerotic plaque instability—analysis in hypercholesterolemic rabbits

Seigo Ishino [a], Takahiro Mukai [b], Noriaki Kume [c,*], Daigo Asano [a], Mikako Ogawa [d], Yuji Kuge [a], Manabu Minami [c], Toru Kita [c], Masashi Shiomi [e], Hideo Saji [a]

[a] *Department of Patho-functional Bioanalysis, Graduate School of Pharmaceutical Sciences, Kyoto University, Japan*
[b] *Department of Biomolecular Recognition Chemistry, Graduate School of Pharmaceutical Sciences, Kyushu University, Japan*
[c] *Department of Cardiovascular Medicine, Graduate School of Medicine, Kyoto University, Japan*
[d] *Laboratory of Genome Bio-Photonics Photon Medical Research Center, Hamamatsu University School of Medicine, Japan*
[e] *Institute for Experimental Animals, Kobe University School of Medicine, Japan*

Received 22 March 2006; received in revised form 30 October 2006; accepted 21 November 2006

Abstract

Lectin-like oxidized LDL receptor-1 (LOX-1), a cell-surface receptor for oxidized LDL (Ox-LDL), has been implicated in vascular cell dysfunction related to atherosclerotic plaque instability, according to cell culture experiments. In the present study, we investigated the relationship between LOX-1 expression and plaque instability in hypercholesterolemic rabbits by immunohistological analyses in vivo. We prepared thirty series of cross sections of the thoracic aorta from six myocardial infarction-prone Watanabe heritable hyperlipidemic (WHHLMI) rabbits (12–24 months), in which seventy atherosclerotic plaques were observed. LOX-1, matrix metalloproteinase-9 (MMP-9), monocyte chemoattractant protein-1 (MCP-1) expression, apoptotic events, plaque instability index (an index of the morphological destabilization of atherosclerotic plaques) and fibromuscular cap thickness in each atherosclerotic plaque were determined by immunohistochemical staining, TUNEL staining and Azan–Mallory staining. LOX-1 expression was positively correlated with the plaque instability index and MMP-9 expression. LOX-1 expression was more prominent in atherosclerotic plaques with thinner fibromuscular cap (<100 μm). Furthermore, LOX-1 expression was shown in the macrophage-rich lipid core area where MCP-1 expression and apoptotic events were prominent. These results indicate that enhanced LOX-1 expression was associated with histologically unstable atherosclerotic plaques in hypercholesterolemic rabbits, suggesting the involvement of LOX-1 in the destabilization of atherosclerotic plaques in vivo.
© 2006 Elsevier Ireland Ltd. All rights reserved.

Keywords: LOX-1; MMP-9; MCP-1; Apoptosis; WHHLMI rabbits

1. Introduction

The disruption of unstable atherosclerotic plaques and subsequent formation of occlusive thrombi are currently recognized as the primary cause of acute coronary syndrome [1–3]. Atherosclerotic plaques with large lipid cores, thin fibromuscular caps, enhanced mononuclear leukocyte accumulation and proinflammatory responses, and expression of matrix metalloproteinases (MMPs) have been suggested to be more susceptible to rupture [4].

Lectin-like oxidized LDL receptor-1 (LOX-1), a type II membrane glycoprotein belonging to the C-type lectin family, acts as a cell-surface receptor for oxidized LDL (Ox-LDL) and mediates several biological effects of Ox-LDL [5]. Previous studies with cultured cells suggest that LOX-1 may play important roles in the pathogenesis of atherosclerosis, such as induced expression of adhesion molecules and chemokines

* Corresponding author. Tel.: +81 75 751 3623; fax: +81 75 751 4094.
E-mail address: nkume@kuhp.kyoto-u.ac.jp (N. Kume).

0021-9150/$ – see front matter © 2006 Elsevier Ireland Ltd. All rights reserved.
doi:10.1016/j.atherosclerosis.2006.11.031

Please cite this article in press as: Ishino S, et al., Lectin-like oxidized LDL receptor-1 (LOX-1) expression is associated with atherosclerotic plaque instability—analysis in hypercholesterolemic rabbits, Atherosclerosis (2007), doi:10.1016/j.atherosclerosis.2006.11.031

for monocytes [6,7], transformation of macrophages into foam cells [8–10], smooth muscle cells apoptosis [11,12] and degradation of extracellular matrix proteins by induction of MMPs [13]. These biological effects mediated by Ox-LDL–LOX-1 interactions would collectively enlarge the lipid core, weaken the fibromuscular cap, and induce proinflammatory responses, resulting in destabilization of atherosclerotic plaques; however, roles of LOX-1 in plaque instability in vivo remain to be determined.

As a hypercholesterolemic rabbit model of spontaneous atherosclerosis, myocardial infarction-prone Watanabe heritable hyperlipidemic (WHHLMI) rabbits (previous strain; Watanabe heritable hyperlipidemic (WHHL) rabbits) have been widely used because the histological characteristics of their atherosclerotic lesions appear to be similar to those in humans [14–17]. In addition, a monoclonal antibody directed to rabbit LOX-1 has been established, and LOX-1 expression by endothelial cells and macrophages in fatty streak lesions has already been reported in WHHL rabbit aortas [18]. LOX-1 expression in advanced atherosclerotic plaques of human carotid arteries has been observed in intimal smooth muscle cells, as well as macrophages and endothelial cells [19].

In the present study, we examined the relationship between LOX-1 expression and histological markers of plaque instability, such as the plaque instability index (an index of morphological destabilized characteristics of atherosclerotic plaques), MMP-9 expression, MCP-1 expression, apoptotic events, and fibromuscular cap thickness in this hypercholesterolemic rabbit model.

2. Methods

2.1. Animals

Six WHHLMI rabbits (12–24 months old: 3.0–3.25 kg body weight) bred at Kobe University were used in the present study. Rabbits were fed standard rabbit chow (type CR-3; Clea Japan Inc., Tokyo, Japan: 120 g/day) and were given water ad libitum. As a control, a Japanese White rabbit (3 month old; Biotec Inc., Saga, Japan: 3.0 kg body weight) was used. All experimental procedures were approved by the Kyoto University Animal Care Committee.

2.2. Preparation of histological sections

Rabbits were sacrificed with an overdose of sodium pentobarbital. The descending thoracic aorta was divided into 5 portions (2 cm segments), after adjacent fat and connective tissue had been removed. These aortic segments were immediately fixed in a solution containing L-(+)-lysine hydrochloride (75 mmol/L) and 4% paraformaldehyde in phosphate buffer (37.5 mmol/L, pH 7.4), and embedded in paraffin. Consecutive 5 μm thick slices were prepared at 1 cm from the end of the 2 cm segments.

2.3. Preparation of a monoclonal antibody directed to rabbit LOX-1

A monoclonal antibody directed to rabbit LOX-1 was established using a standard hybridoma technique. Polypeptide corresponding to the amino acid numbers between 150 and 171 of the rabbit LOX-1 (extracellular domain) was used as an antigen to immunize mice. A monoclonal antibody by which COS-7 cells transfected with rabbit LOX-1 cDNA, but not untransfected wild-type COS-7 cells, were able to be immunochemically stained, was utilized.

2.4. Histological analysis

Serial sections were subjected to immunostaininig for LOX-1, MMP-9, MCP-1 and cell type marker antigens. A monoclonal antibody for MMP-9 (mouse IgG) was obtained from Daiichi Fine Chemical Corp., Toyama, Japan. A monoclonal antibody for MCP-1 (mouse IgG) was obtained from BD Biosciences Inc., San Jose, CA, USA [20]. Monoclonal antibodies for a rabbit macrophage-specific antigen (RAM-11, mouse IgG) and smooth muscle actin (1A4, mouse IgG) were obtained from Dako Corp., Santa Barbara, CA, USA. Immunohistostaining was carried out using a Dako Envision+kit (Dako) with hematoxylin counterstaining. Immunohistochemical staining with an anti-von Willebrand factor (vWf) polyclonal antibody (goat IgG, Atlantic Antibodies, Stillwater, MN), which cross-reacts with rabbit vWf, was carried out to identify rabbit endothelial cells by use of a Dako Envision/AP kit (Dako) followed by hematoxylin counterstaining. Immunostaining with subclass-matched irrelevant IgG served as a negative control.

Azan–Mallory staining was performed with standard procedures. Apoptotic nuclei were determined by terminal deoxyribonucleotide transferase (TdT)-mediated nick-end labeling (TUNEL) using a commercially available kit (in situ apoptosis detection kit, Trevigen Inc., Gaithersburg, MD, USA).

2.5. Definition of atherosclerotic plaques

In atherosclerotic plaques, the lipid core was defined as a layer more than 100 μm thick consisting of macrophage foam cells and extracellular lipid deposits, which was measured using a VHX Digital Microscope (Keyence Corp., Osaka, Japan). Fibromuscular caps were defined as areas consisting of smooth muscle cells and collagen fibers, which cover the lipid core. The systematic structure of an atherosclerotic plaque is shown in Fig. 1. Typical unstable plaques contained predominantly macrophages or large lipid cores, with a thin or scarcely perceivable fibromuscular cap consisting of smooth muscle cells and collagen fibers. On the other hand, typical stable plaques contained scattered macrophages and lipid cores in deep intimal areas with a thicker fibromuscular cap. The atherosclerotic plaques were classified into two groups based on fibromuscular cap thickness (cut-off value, 100 μm)

Please cite this article in press as: Ishino S, et al., Lectin-like oxidized LDL receptor-1 (LOX-1) expression is associated with atherosclerotic plaque instability—analysis in hypercholesterolemic rabbits, Atherosclerosis (2007), doi:10.1016/j.atherosclerosis.2006.11.031

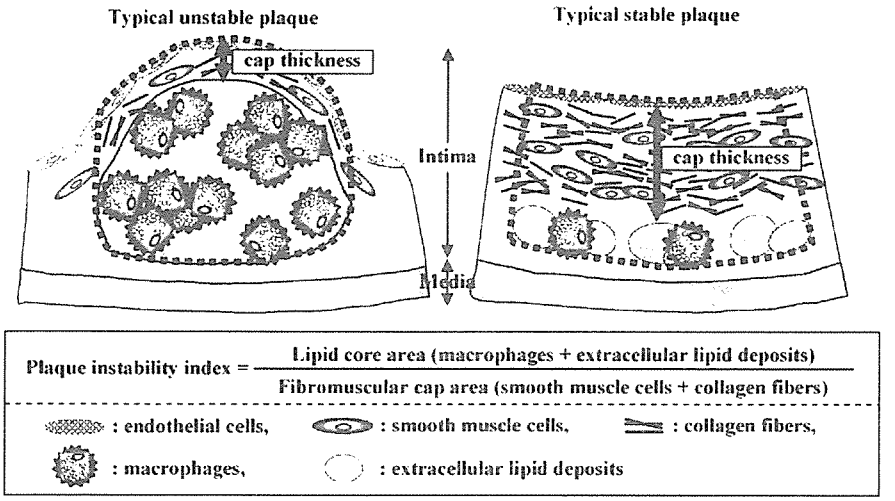

Fig. 1. Schematic illustration of a typical atherosclerotic plaque and its components described in the text. The area within dotted lines shows typical unstable plaques (left) and typical stable plaques (right). In each atherosclerotic plaque, the ratio of the lipid core area (macrophages and extracellular lipid deposits) to the fibromuscular cap area (smooth muscle cells and collagen fibers covering the lipid core area) was defined as a 'plaque instability index'. Fibromuscular cap thickness was measured at the point of the thickest lipid core with clear demarcation of the fibromuscular cap-lipid core interface.

measured at the point of the thickest lipid core with a clear demarcation of the fibromuscular cap-lipid core interface as shown in Fig. 1.

2.6. Quantitative analysis

Lesion component areas were quantitatively evaluated with the microscope. In each section with Azan–Mallory staining, we examined all atherosclerotic plaques and measured the ratio of the LOX-1-positive area to the entire area of the plaque (LOX-1 expression density). Using the same method, MMP-9 expression density was determined. As an index of morphologically destabilized characteristics, the ratio of the lipid core area (macrophages and extracellular lipid deposits) to the fibromuscular cap area (smooth muscle cells and collagen fibers covering the lipid core area) was calculated from the results of Azan–Mallory staining, as well as immunostaining for macrophages (RAM-11) and smooth muscle cells (1A4). This ratio (lipid core area/fibromuscular cap area) was defined as a 'plaque instability index' in each atherosclerotic plaque. We measured blue region as collagen fibers or other extracellular matrix proteins, and extracellular vacuoles and lacunae as extracellular lipid deposits in Azan–Mallory-stained sections [21,22], and RAM-11-positive areas as macrophages and 1A4-positive areas as smooth muscle cells in immunostained sections. In each section, the plaque instability index, MMP-9 expression density and fibromuscular cap thickness were compared with LOX-1 expression density.

2.7. Statistical analyses

Values were expressed as the mean ± S.D. Statistical analysis was performed with the Mann–Whitney *U* test for comparing LOX-1 expression density. Correlation coefficients were assessed with Spearman rank correlation coefficients. Statistical significance was defined as $P < 0.0001$.

3. Results

3.1. Composition of atherosclerotic plaque and MMP-9 expression

In the thoracic aorta of WHHLMI rabbits, we analyzed seventy atherosclerotic plaques found in thirty series of sections from six animals (five segments per rabbit). Fig. 2 shows typical images of unstable (left two columns) and stable (right two columns) atherosclerotic plaques with Azan–Mallory and immunohistochemical staining. Fig. 3 shows higher magnification images of each staining corresponding to the area indicated as a square in Fig. 2 V. The unstable plaques (left two columns) looked similar to rupture-prone unstable human plaques which consist of a large lipid core with abundant macrophages and extracellular lipid deposits, accompanied by a thin fibromuscular cap with relatively few smooth muscle cells scattered in the superficial region (Figs. 2 and 3). MMP-9 expression was mainly observed in RAM-11-positive areas (Figs. 2E, F, I, J and 3B, C). On the other hand, stable plaques (right two columns) showed typical characteristics such as few macrophages, less extracellular lipid deposits and a thicker fibromuscular cap (Fig. 2). Less prominent MMP-9 expression, as well as a larger number of smooth muscle cells and collagen fibers or more extracellular matrix was observed (Fig. 2G, H, O, P, W, X). MMP-9 signals were undetectable in aortic sections from normocholesterolemic control rabbits (data not shown).

Please cite this article in press as: Ishino S, et al., Lectin-like oxidized LDL receptor-1 (LOX-1) expression is associated with atherosclerotic plaque instability—analysis in hypercholesterolemic rabbits, Atherosclerosis (2007), doi:10.1016/j.atherosclerosis.2006.11.031

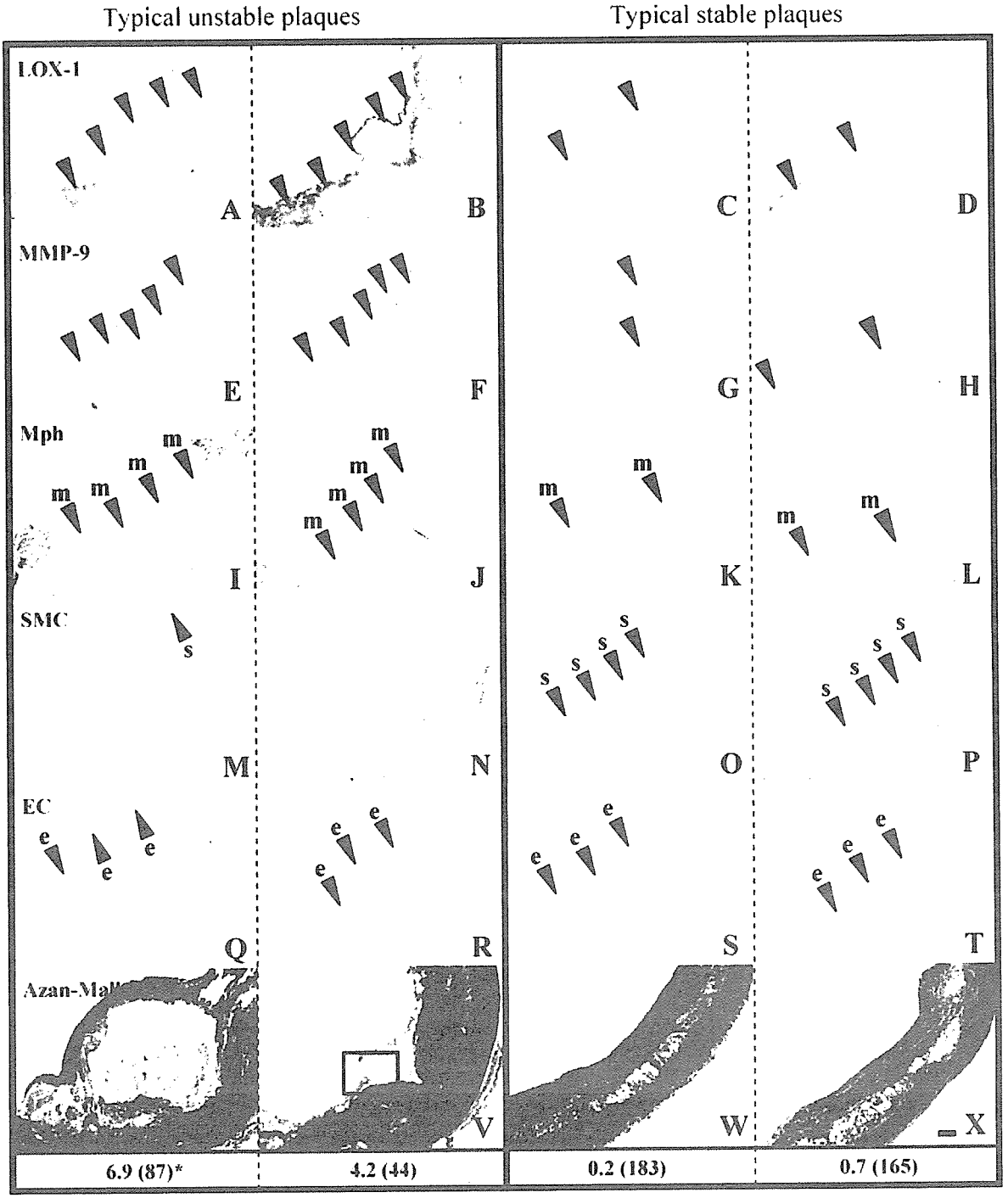

Fig. 2. Photomicrographs of atherosclerotic lesions in the thoracic aorta of WHHLMI rabbits showed typical unstable (left two columns) and stable (right two columns) atherosclerotic plaques. Immunohistochemical staining for LOX-1 (A to D), MMP-9 (E to H), macrophages (I to L), smooth muscle cells (M to P), and endothelial cells (Q to T) and Azan–Mallory staining (U to X). *The values in the lowest row show the plaque instability index (fibromuscular cap thickness) in each atherosclerotic plaque. Bar = 100 μm, magnification × 30. (m: macrophages; s: smooth muscle cells; e: endothelial cells).

3.2. LOX-1 expression and composition of plaques

The distribution of LOX-1 in atherosclerotic plaques was determined by immunohistochemical staining of serial sections with an anti-rabbit LOX-1 monoclonal antibody. As reported previously [18], LOX-1 was intensively expressed in the intima of atherosclerotic lesions, and endothelial cells and macrophages were stained positively for LOX-1

Please cite this article in press as: Ishino S, et al., Lectin-like oxidized LDL receptor-1 (LOX-1) expression is associated with atherosclerotic plaque instability—analysis in hypercholesterolemic rabbits, Atherosclerosis (2007), doi:10.1016/j.atherosclerosis.2006.11.031

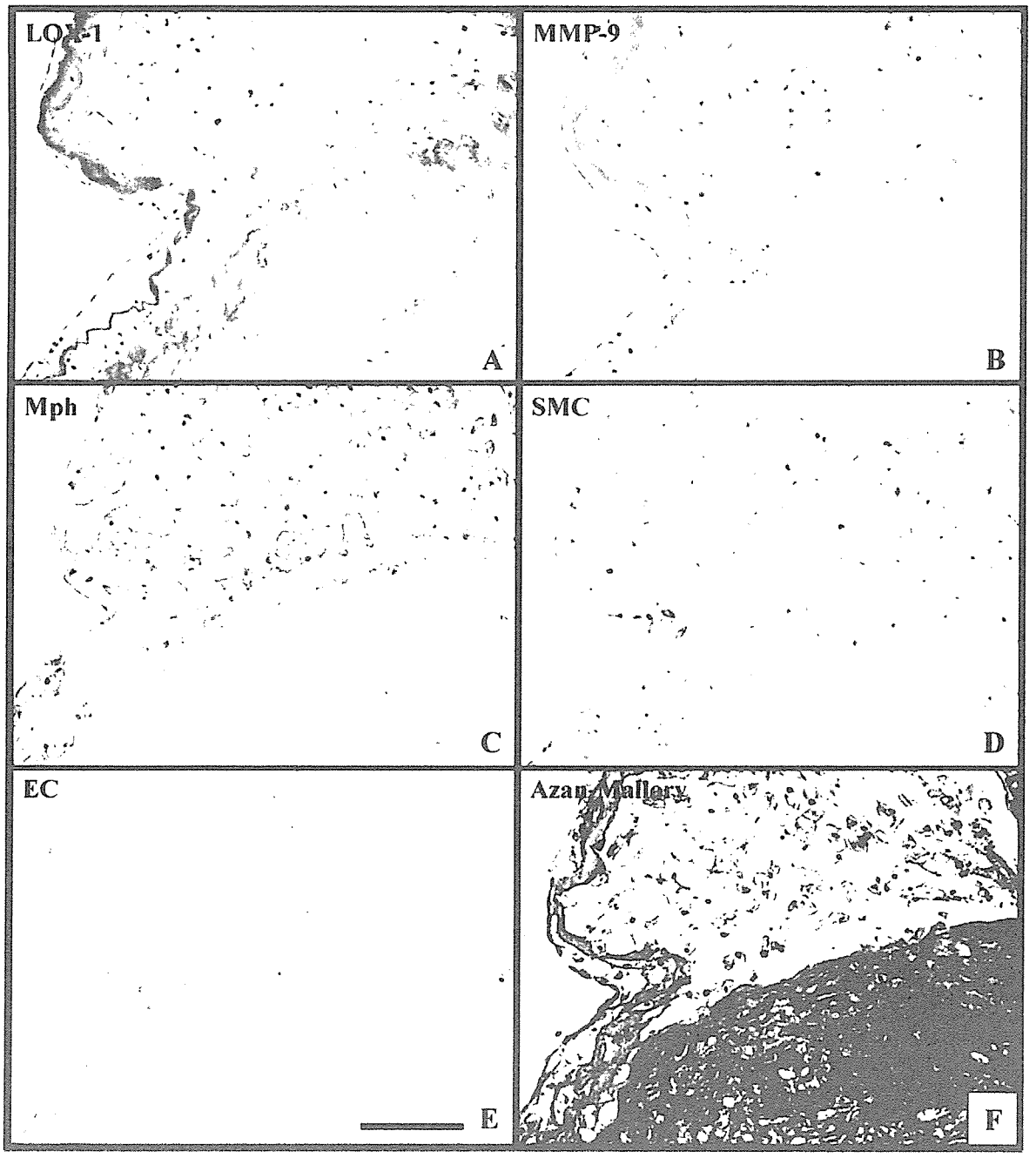

Fig. 3. Higher magnification images of unstable plaques corresponding to the area indicated as a square in Fig. 2 V. Immunohistochemical staining for LOX-1 (A), MMP-9 (B), macrophages (C), smooth muscle cells (D), and endothelial cells (E), and Azan–Mallory staining (F). Bar = 100 μm, magnification ×150.

(Fig. 2A–D, I–L, Q–T and 3A, C, E). In addition, intimal smooth muscle cells also prominently expressed LOX-1 (Figs. 2C, D, O, P and 3A, D) as previously reported in advanced human atherosclerotic plaques [19], although LOX-1 expression levels varied among atherosclerotic plaques (Fig. 2A–D). LOX-1 immunostaining was not observed in aortic sections from normocholesterolemic control rabbits (data not shown).

3.3. Correlation of LOX-1 expression density with plaque instability index or MMP-9 expression density

Using the histological images, we carried out quantification analyses as described in the Methods. LOX-1 expression density was positively correlated with the plaque instability index ($R = 0.74$, $P < 0.0001$, Fig. 4A) in this animal model of atherosclerosis. Furthermore, LOX-1 expression density

Please cite this article in press as: Ishino S, et al., Lectin-like oxidized LDL receptor-1 (LOX-1) expression is associated with atherosclerotic plaque instability—analysis in hypercholesterolemic rabbits, Atherosclerosis (2007), doi:10.1016/j.atherosclerosis.2006.11.031

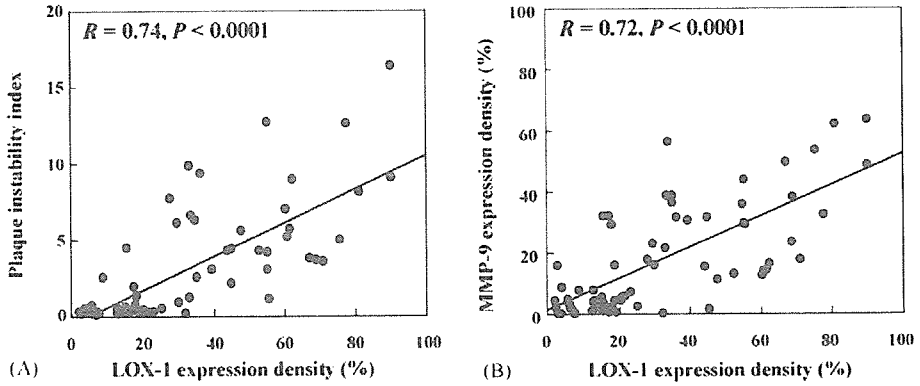

Fig. 4. Correlation of LOX-1 expression density with plaque instability index (A), or MMP-9 expression density (B), in atherosclerotic plaques in the thoracic aorta of WHHLMI rabbits ($n = 70$). Regression analyses demonstrated a positive correlation between LOX-1 expression density and plaque instability index ($R = 0.74$, $P < 0.0001$), as well as between LOX-1 expression density and MMP-9 expression density ($R = 0.72$, $P < 0.0001$).

positively correlated with MMP-9 expression density ($R = 0.72$, $P < 0.0001$, Fig. 4B), thus suggesting roles for LOX-1 in MMP expression, as well as apoptosis and foam cell transformation, as shown in cultured cells.

3.4. Classification of atherosclerotic plaques based on fibromuscular cap thickness

Atherosclerotic plaques were classified into two groups based on fibromuscular cap thickness (cut off value: 100 μm). Levels of LOX-1 expression density were significantly higher in the atherosclerotic plaques with thinner fibromuscular caps than those with thicker ones (51.1 ± 21.1 versus 17.1 ± 13.5 %, $P < 0.0001$).

3.5. LOX-1/MCP-1 expression and apoptotic events in atherosclerotic lesions

Fig. 5 shows LOX-1 and MCP-1 expression, and apoptotic events in unstable plaques. In the lipid core area, MCP-1 expression and TUNEL-positive nuclei were prominent mainly in macrophages (foam cells), in which LOX-1 expression was prominent. On the other hand, neither LOX-1 nor MCP-1 expression, nor TUNEL-positive cells were detectable in the fibromuscular cap area. Thus, LOX-1 expression appeared to be co-localized with MCP-1 expression and TUNEL-positive cells in macrophages (foam cells) located in the lipid core area. Neither MCP-1 expression nor TUNEL-positive nuclei were detectable in aortic sections from normocholesterolemic control rabbits (data not shown).

4. Discussion

We investigated the LOX-1 expression in association with histological markers of plaque instability, such as the plaque instability index, MMP-9 expression and fibromuscular cap thickness, and examined the co-localization of LOX-1 expression with MCP-1 expression and apoptotic events in hypercholesterolemic rabbits.

To evaluate the morphological destabilization of atherosclerotic plaques, we proposed a 'plaque instability index' calculated as the ratio between the two histological areas in atherosclerotic plaques: the lipid core area (macrophages plus extracellular lipid deposits) and the fibromuscular cap area (smooth muscle cells plus collagen fibers). As a histological index of atherosclerotic plaque, Shiomi et al. previously proposed a 'vulnerability index', calculated as the ratio between the two histological components (lipid and fibromuscular components) in the entire intima [21]. Compared to the vulnerability index, the plaque instability index would more directly reflect the thickness of the fibromuscular cap and the plaque instability because it was not calculated from the whole intimal area, but from the atherosclerotic plaque area. This plaque instability index was significantly correlated with LOX-1 expression density.

MMP-9, also known as gelatinase B or 92 kDa type IV collagenase, has been found to be prominently expressed in unstable atherosclerotic plaques in humans. Accordingly, MMP-9 has been suggested to be involved in the rupture of atherosclerotic plaques [23,24]. It has been reported that LOX-1-mediated uptake of Ox-LDL modulates the expression and activity of MMPs in cultured endothelial cells [13]. However, it remained unknown whether LOX-1 expression is associated with MMP-9 expression in vivo. This study showed, for the first time, that LOX-1 expression density was significantly correlated with MMP-9 expression density in atherosclerotic plaques. Thus, LOX-1 is also responsible for the Ox-LDL-induced expression of MMPs and thereby, the destabilization of plaques.

Because a fibromuscular cap thickness less than 100 μm has been reported as a marker of susceptibility to plaque rupture [25], we used this cut-off value to classify atherosclerotic plaques into two groups. According to this cut-off value, LOX-1 expression density was found to be significantly higher in the thinner fibromuscular cap group (<100 μm) than thicker cap group (>100 μm).

Please cite this article in press as: Ishino S, et al., Lectin-like oxidized LDL receptor-1 (LOX-1) expression is associated with atherosclerotic plaque instability—analysis in hypercholesterolemic rabbits, Atherosclerosis (2007), doi:10.1016/j.atherosclerosis.2006.11.031